

CHARACTERIZATION OF THE  
GRAYBURG RESERVOIR OF THE  
MOBIL UNIVERSITY UNIT 15/16 IN DUNE FIELD,  
CRANE COUNTY, TEXAS

by

D. G. Bebout, D. A. Leary, F. J. Lucia, C. R. Hocott, and S. Schmidt

An interim report on a continuing project funded by:

The State of Texas and  
The University of Texas System

July 31, 1985

Bureau of Economic Geology  
W. L. Fisher, Director  
The University of Texas at Austin  
Austin, Texas 78713

## CONTENTS

INTRODUCTION . . . . .	1
Incentives and objectives . . . . .	1
Regional setting . . . . .	1
Production . . . . .	5
Mobil University Unit 15/16 . . . . .	5
STRATIGRAPHY AND WELL LOG CORRELATION . . . . .	10
DOLOMITE FACIES . . . . .	15
Introduction . . . . .	15
Facies descriptions . . . . .	15
Vertical facies distribution . . . . .	27
Lateral facies distribution . . . . .	29
Depositional environments . . . . .	37
DIAGENESIS . . . . .	39
Porosity/permeability . . . . .	41
PRODUCTION STUDIES -- DUNE FIELD UNIT 15/16 . . . . .	44
CONCLUSIONS . . . . .	48
REFERENCES . . . . .	49

## FIGURES

1. Estimated original oil in place in Texas . . . . .	2
2. Cumulative production of oil from Texas through 1982 . . . . .	2
3. Cumulative production of oil from the Permian Basin through 1982 . . . . .	2
4. Cumulative production of oil from carbonate reservoirs through 1982 . . . . .	2
5. Principal Paleozoic oil-bearing units of North and West Texas . . . . .	3
6. Location of the cross section across the Central Basin Platform . . . . .	3

7.	Structural cross section across the Central Basin Platform. . . . .	4
8.	Location of University Lands in the Permian Basin . . . . .	4
9.	San Andres/Grayburg fields, Permian Basin, Texas . . . . .	6
10.	Outline of Dune Field showing the location of the study area . . . . .	6
11.	Well log and core control in the study area . . . . .	6
12.	Structure on the top of the Grayburg Formation. . . . .	8
13.	Cumulative production through 1982 from sections 15 and 16 . . . . .	8
14.	Initial-potential map prepared using older wells drilled prior to waterflooding . . . . .	9
15.	Gamma ray/sonic log of the San Andres, Grayburg, and Queen section in the Mobil University No. 1557 . . . . .	11
16.	Index map of the study area showing the location of the log correlation cross sections . . . . .	13
17.	Pisolite grainstone facies comprising pisolite grainstone, laminated mudstone, and algal laminated mudstone facies . . . . .	17
18.	Ooid and pellet grainstone facies . . . . .	19
19.	Fusulinid wackestone facies . . . . .	21
20.	Sponge-algal framestone facies . . . . .	23
21.	Siltstone facies . . . . .	25
22.	Index map of the study area showing location of the detailed facies cross section . . . . .	28
23.	Detailed facies cross section . . . . .	28
24.	Cross plot of neutron porosity vs. resistivity using wells from the west half of the study area. . . . .	30
25.	Cross plot of sonic travel time vs. neutron porosity using wells from the east half of the study area . . . . .	30
26.	Thickness of the MA Dolomite . . . . .	32
27.	Thickness of the A Siltstone . . . . .	32
28.	Thickness of the AB Dolomite . . . . .	33
29.	Thickness of the BC Dolomite . . . . .	33

30.	Thickness of the CZ Dolomite . . . . .	34
31.	Thickness of the Z Siltstone . . . . .	34
32.	Thickness of the ZY Siltstone . . . . .	35
33.	Thickness of the Y Siltstone . . . . .	35
34.	Thickness of the YD Dolomite . . . . .	36
35.	Thickness of the DX Dolomite . . . . .	36
36.	Interpreted depositional environments of the middle unit . . . . .	38
37.	Interpreted depositional environments of the upper unit . . . . .	38
38.	Porosity distribution of the pellet grainstone of the CZ Dolomite in the Mobil University No. 1535 . . . . .	43
39.	Porosity distribution of the ooid grainstone of the AB Dolomite in the Mobil University No. GG4 . . . . .	43
40.	Porosity distribution of the fusulinid wackestone of the MA Dolomite in the Mobil University No. 1535 . . . . .	43
41.	Porosity distribution of the algal framework of the MA Dolomite in the Getty No. 2217 . . . . .	43
42.	Porosity distribution of the crinoid-bryozoan packstone and crinoid-pellet packstone of the MA Dolomite in the Mobil University No. 1540 . . . . .	43
43.	Porosity/permeability cross plot of the pellet grainstone facies . . . . .	45
44.	Porosity/permeability cross plot of the sponge-algal framestone facies . . . . .	45
45.	Porosity/permeability cross plot of the crinoid-bryozoan packstone facies . . . . .	45
46.	Porosity/permeability cross plot of the fusulinid wackestone facies . . . . .	45
47.	Cumulative production from wells drilled prior to 1958 in sections 15 and 16 . . . . .	46
48.	Cumulative production from wells drilled since 1958 . . . . .	46
49.	Cumulative production of oil and water and volume of water injected from 1977 to 1985 from wells in sections 15 and 16 . . . . .	47
50.	Production behavior of Mobil University 1531 and water injection in a nearby well . . . . .	47
51.	Production behavior of Mobil University 1520 and water injection in a nearby well . . . . .	47

## INTRODUCTION

### Incentives and Objectives

A project was initiated by the Bureau of Economic Geology in 1981 to investigate the distribution and nature of oil production in Texas. Approximately 500 reservoirs having a cumulative production of more than 10 million barrels of oil each were included in this study; these reservoirs have produced more than 71 percent of the total Texas production. These larger reservoirs were grouped into 47 plays based on the original depositional setting of the rocks and source and on reservoir and trap characteristics. Twenty-seven of these plays located in the Paleozoic basins of North and West Texas account for 73 percent of the total in-place oil in the state. Most of the Paleozoic production is from dolomite reservoirs. Results of this initial reservoir characterization project by the Bureau are summarized in the "Atlas of Major Texas Oil Reservoirs" (Galloway et al., 1983).

Reservoirs producing from the San Andres/Grayburg Formations were selected for study because of their high cumulative production and low recovery efficiencies (30 percent average). For example, in Texas, 51 percent (80 billion barrels) of the original oil in place and 43 percent (46 billion barrels) of the cumulative production are from the Permian Basin (Figs. 1 and 2). Within the Permian Basin, 83 percent (16.6 billion barrels) of the cumulative production is from carbonates (Fig. 3), and 46 percent (7.7 billion barrels) of this is from San Andres/Grayburg reservoirs (Fig. 4). Therefore, San Andres/Grayburg reservoirs are major contributors to Texas oil production (17 percent of the total cumulative production of Texas) (Fig. 5). Better geological definition of reservoirs incorporated into engineering models and studies should lead to more efficient development of secondary and tertiary recovery methods.

### Regional Setting

The major faulting that formed the Central Basin Platform, Delaware Basin, and Midland Basin occurred during the late Paleozoic (Figs. 6 through 8). The Delaware Basin

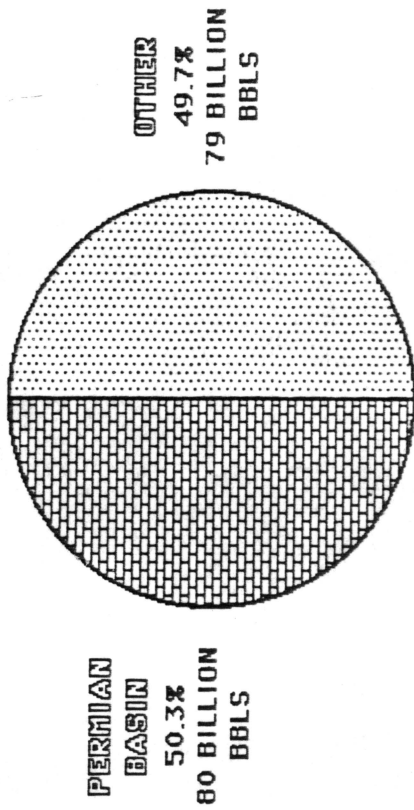


Figure 1. Estimated original oil in place in Texas. More than 50 percent is from the Permian Basin.

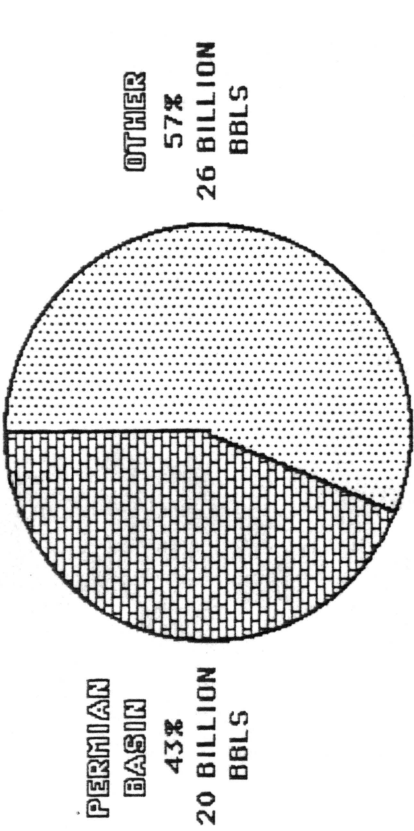


Figure 2. Cumulative production of oil from Texas through 1982.

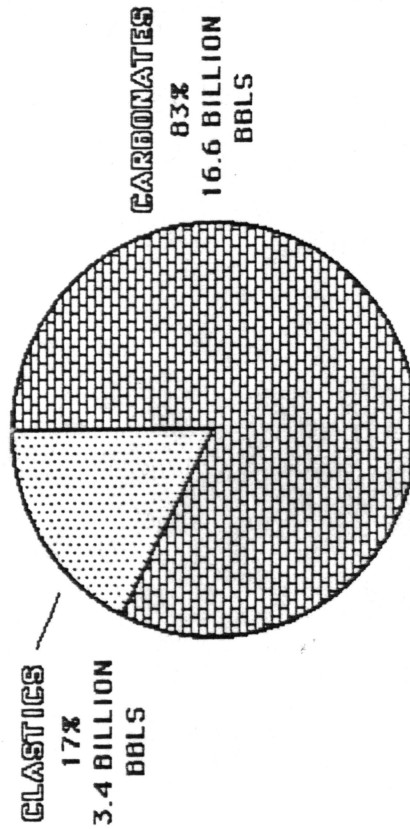


Figure 3. Cumulative production of oil from the Permian Basin through 1982, showing the dominance of carbonate reservoirs.

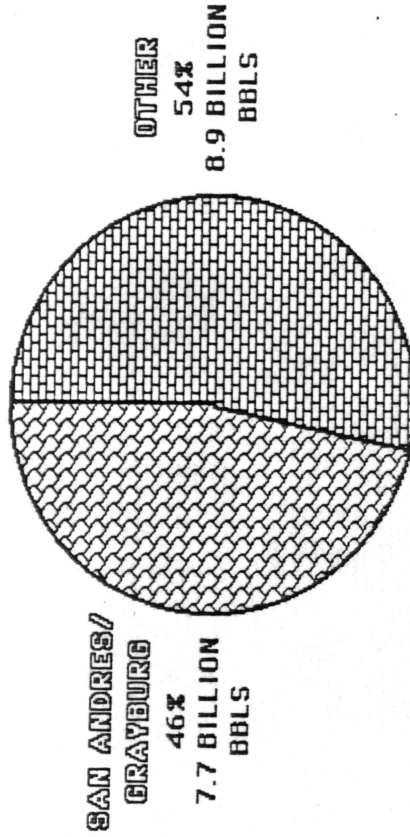


Figure 4. Cumulative production of oil from carbonate reservoirs through 1982. San Andres/Grayburg reservoirs account for almost half of the production from carbonate reservoirs.

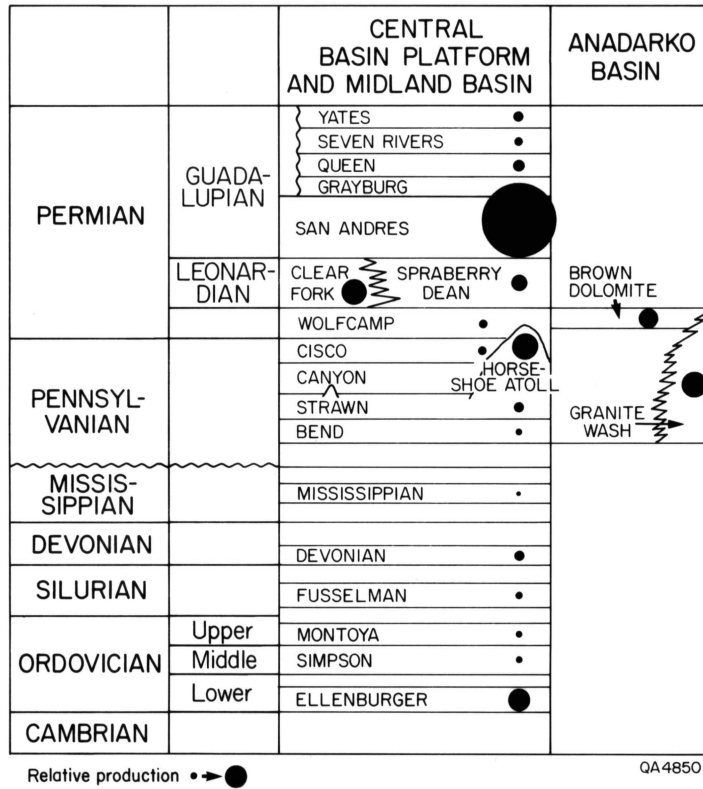


Figure 5. Principal Paleozoic oil-bearing units of North and West Texas. From Galloway et al. (1983).

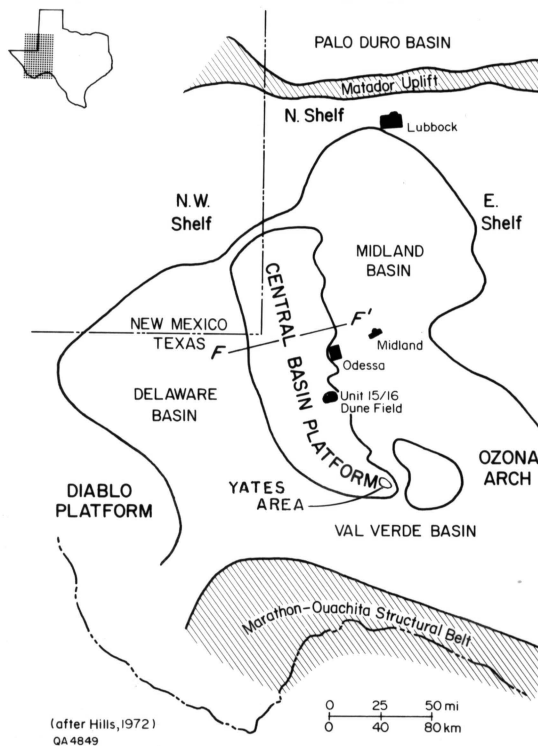


Figure 6. Location of the cross section across the Central Basin Platform.

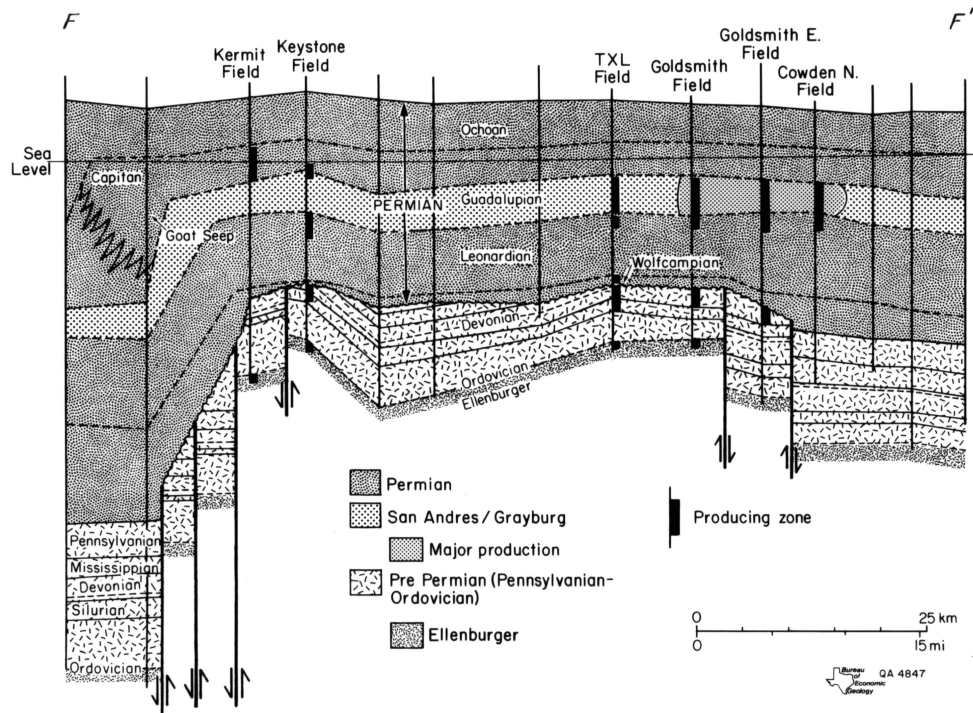


Figure 7. Structural cross section across the Central Basin Platform.

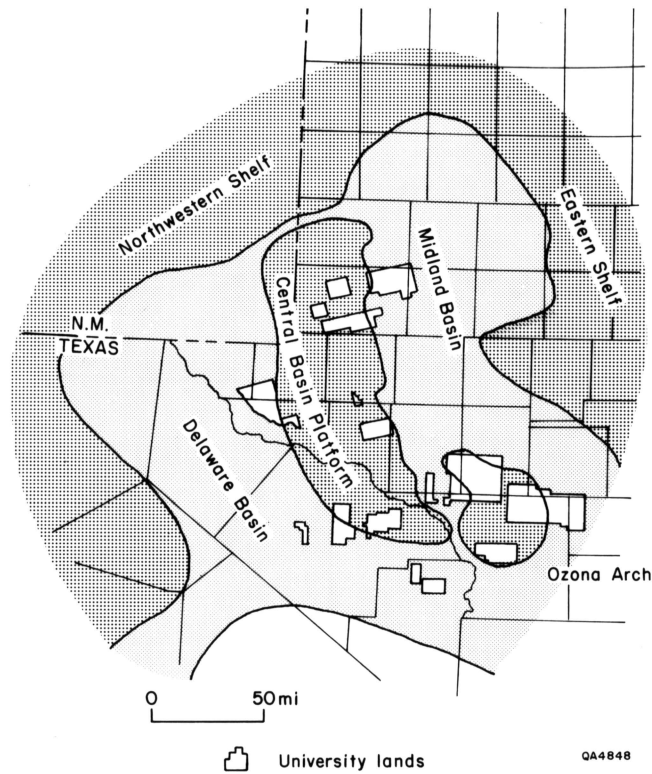


Figure 8. Location of University Lands in the Permian Basin.

when originally formed was greater than 5,000 feet deep; in contrast, the Midland Basin was generally less than 2,000 feet deep. Although both basins were gradually filled during the Permian, the Midland Basin continued to be considerably shallower than the Delaware Basin. Therefore, the depositional settings around these basins are expected to have been significantly different from one another.

Oil in the Permian Basin is produced from six major San Andres/Grayburg plays (Galloway et al., 1983). These plays, Northwestern Shelf Permian Carbonates, Eastern Shelf Permian Carbonates, Northern Central Basin Platform, Southern Central Basin Platform, Yates Area, and Ozona Arch, are all located around the Midland Basin (Fig. 9).

### Production

San Andres/Grayburg production was initiated in 1925 in the McCamey Field along the southern Central Basin Platform; other fields were discovered in the late 1920's, and by the 1930's most of the reservoirs had been discovered.

The discovery well of the Dune Field was completed on January 9, 1938. Since that time, 900 completions have been made in the 22,000-acre area. The 300-foot-thick pay section occurs at an average depth of 3,300 feet. Connate water saturation is 23 percent, and the oil has a gravity of API 34. Water injection was first permitted by the Railroad Commission of Texas on October 13, 1959.

The original oil in place is estimated to have been 590 million barrels; the estimated ultimate recovery (calculated at 28 percent) is 164 million barrels, and 149 million barrels have already been produced.

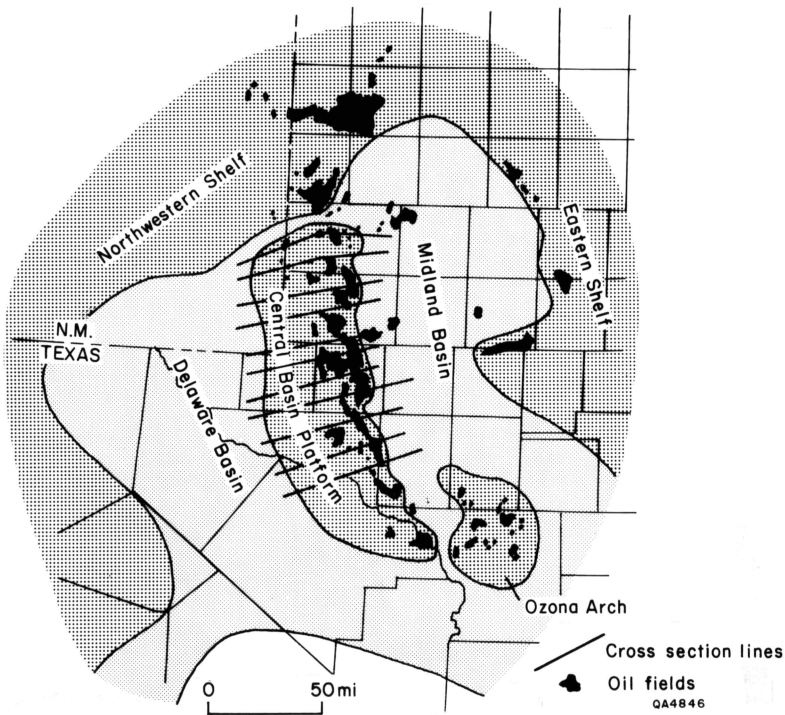


Figure 9. San Andres/Grayburg fields, Permian Basin, Texas.

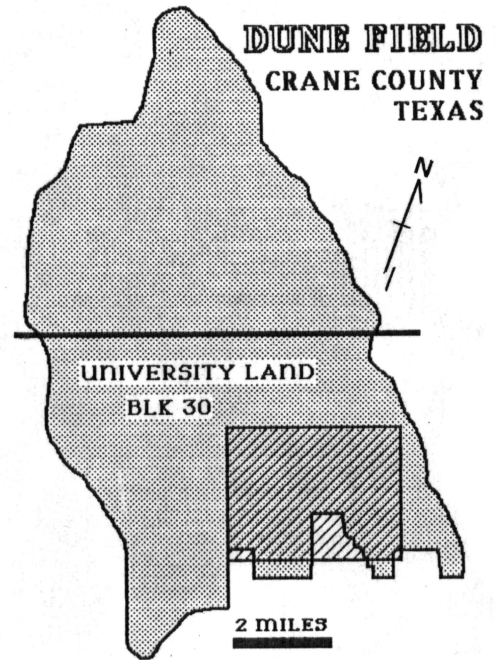


Figure 10. Outline of the Dune Field showing the location of the study area in University Lands Block 30.

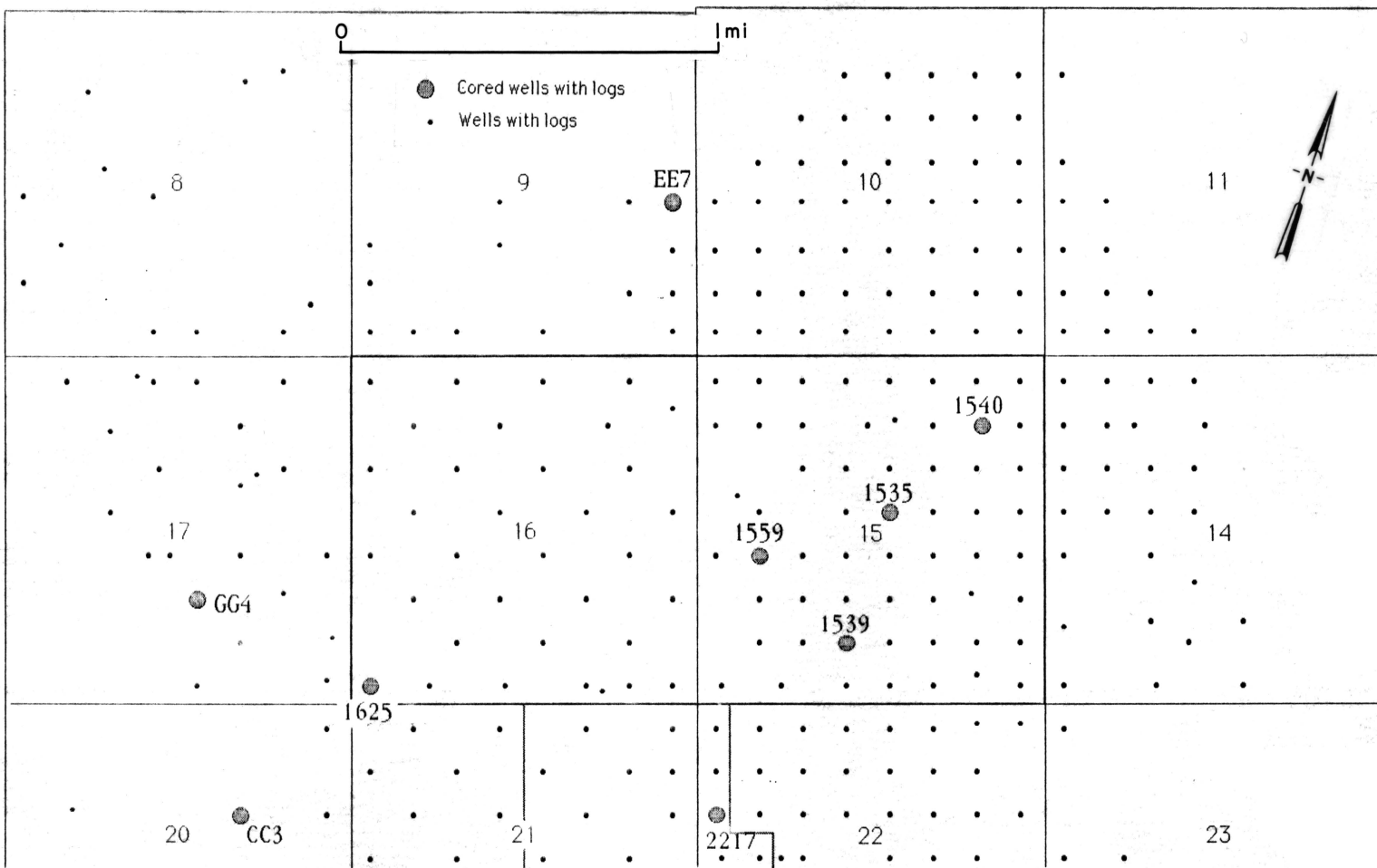


Figure 11. Well-log and core (numbered large dots) control in the study area comprising the Mobil University Unit 15/16 and adjoining sections.

## Mobil University Unit 15/16

Mobil University Unit 15/16, Dune Field, Crane County, Texas (Fig. 10), was selected as a pilot study because of operator willingness to make cores from closely spaced wells available to the Bureau. Cores of the entire producing section were released to the project from four wells within the unit (Mobil 1625, 1539, 1535, and 1540); cores from five wells near the unit were available (Mobil GG4, Mobil CC3, Getty 2217, and Gulf EB9 and EE7). Logs were available from more than 230 wells (Fig. 11). Mobil, Getty, and Gulf also provided logs and core analyses from these wells. The University Lands Office in Midland had logs, core analyses, production data, and maps of University Lands areas in addition to logs from wells near University Lands. These files and those of the Railroad Commission of Texas in Austin yielded production data and well locations.

Unit 15/16 lies on the northeast side of a low-relief structure that dips gently to the northeast into the Midland Basin (Fig. 12). The highest part of the structure (-400 feet) is at the southwestern side of section 16; section 15 is lower on the structure at -500 to -750 feet. Calculations of total cumulative production indicate that 9.7 million barrels have been produced from section 15 and only 1.9 million barrels have been produced from section 16 (Fig. 13). This difference in production is supported by the map showing the initial production rates on older wells drilled prior to beginning waterflood operations (Fig. 14). Wells with high initial production and no water are located along a northwest-to-southeast trend through the center of section 15. The line that separates the area of high IPs and no water production from that of low IPs and water production cuts the northeast corner of section 16 and the southwest corner of section 15. From these preliminary maps it was concluded that significant differences in the depositional facies and related porosity and permeability occur between these two sections. These differences are responsible for controlling initial production characteristics of the unit.

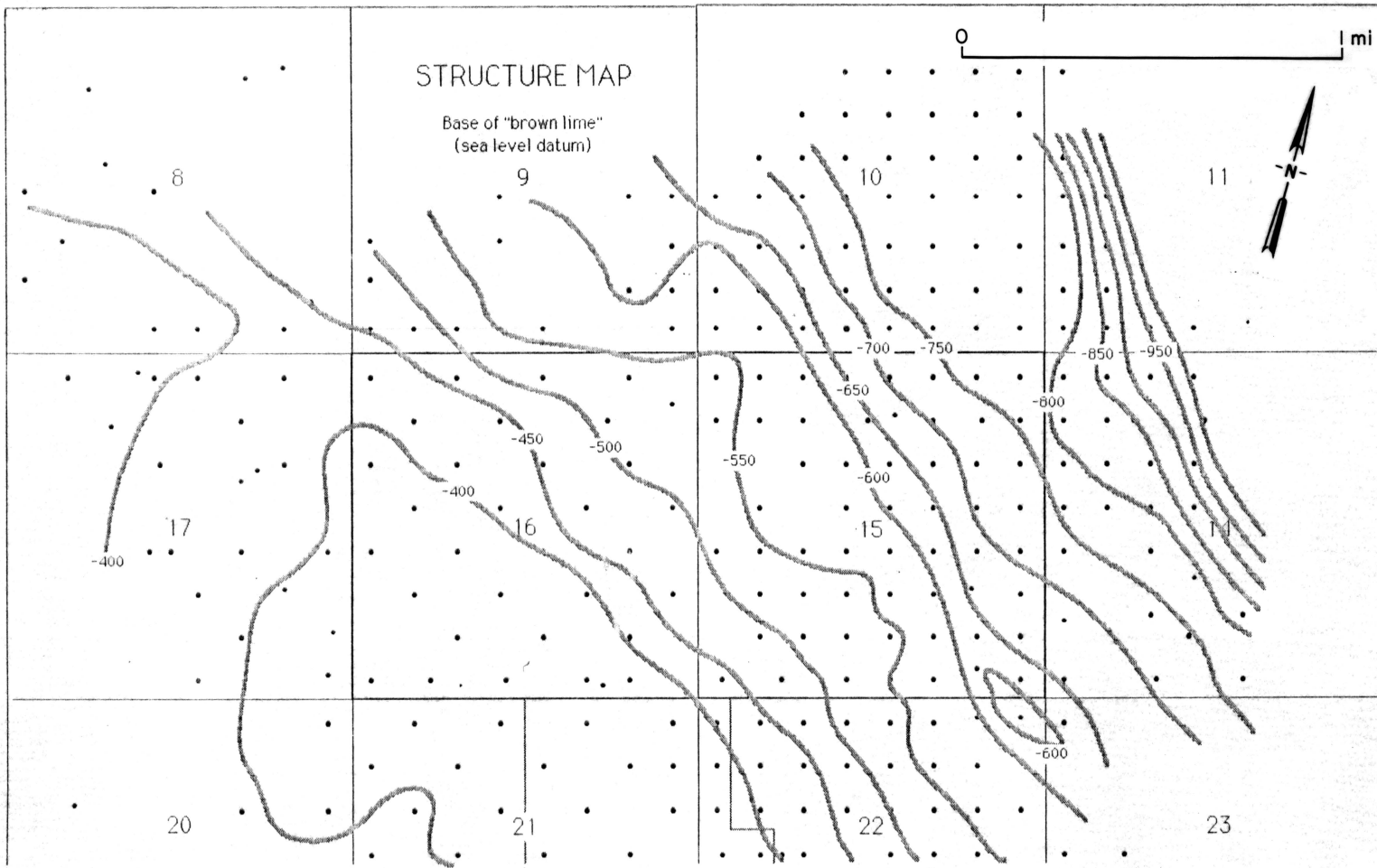


Figure 12. Structure on the top of the Grayburg Formation (Fig. 15).

**TEXAS UNIVERSITY UNIT 15/16  
TOTAL PRODUCTION**

	<b>16</b>	<b>15</b>
	1.9 million barrels	9.7 million barrels
	34 wells	56 wells

Figure 13. Cumulative production through 1982 from sections 15 and 16.

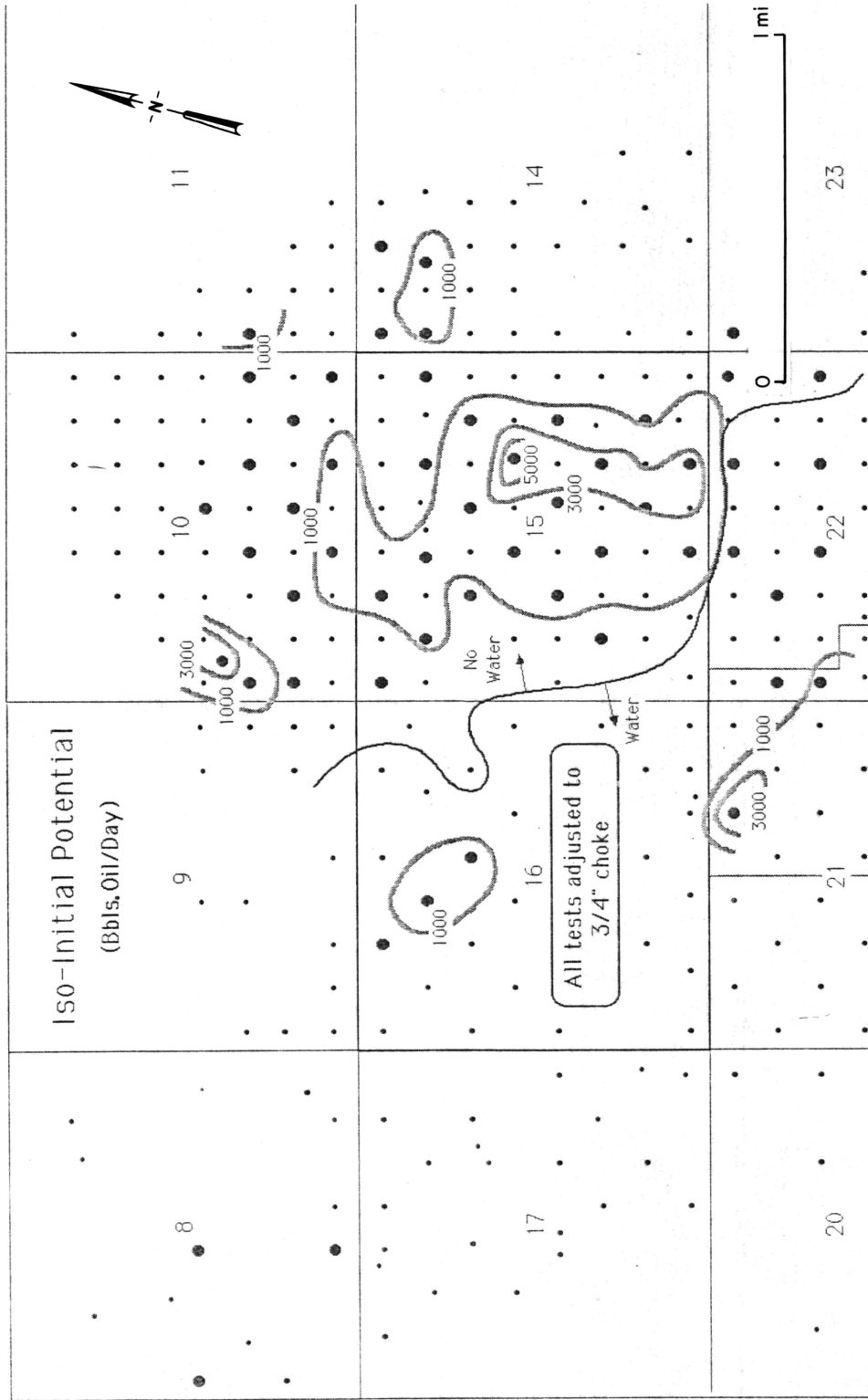


Figure 14. Initial-potential map prepared using older wells drilled prior to waterflooding.

## STRATIGRAPHY AND WELL LOG CORRELATION

Three formations--the Queen, Grayburg, and San Andres--have been identified in the study area, but the exact placement of the boundaries between them is arbitrary and of only local value. The type sections of the Queen, Grayburg, and San Andres are from outcrop exposures and wells many miles away; precise correlation from these type sections to the subsurface is difficult because of lack of recognizable marker beds having lateral continuity and lack of preserved fossils. Many of the operational picks by companies are based on vertical facies relationships in a particular field; however, these changes are expected to occur at different horizons and geological times depending upon the position on the platform. Therefore, operational tops of these units have been selected based on regionally correlatable log patterns supported by some knowledge of lithology and diagenetic patterns (Fig. 15). The base of the Queen was picked at the base of the Brown Lime, a stratigraphic marker carried from the McElroy Field to the south, and is characterized by approximately 300 feet of interbedded anhydritic dolomite and siltstone; anhydrite is abundant as cement and nodules, porosity is lacking, and the gamma-ray log reads less than 10 API units. The contact of the Queen with the underlying Grayburg is transitional, with the anhydrite gradually decreasing into the Grayburg and the siltstone beds becoming thinner and more widely spaced. Porosity is low in the upper 100 feet of the Grayburg and relatively high in the remaining lower 200 feet, which comprises the producing section of the Dune Field. Vuggy and dolomitic intercrystalline porosity are well developed in the Grayburg. The contact between the Grayburg and the underlying San Andres is picked at the low-gamma shoulder (M marker), which signifies the change from the upper dolomite having intercrystalline porosity to the tight matrix of the lower dolomite. This abrupt contact probably indicates the boundary of a significant diagenetic event.

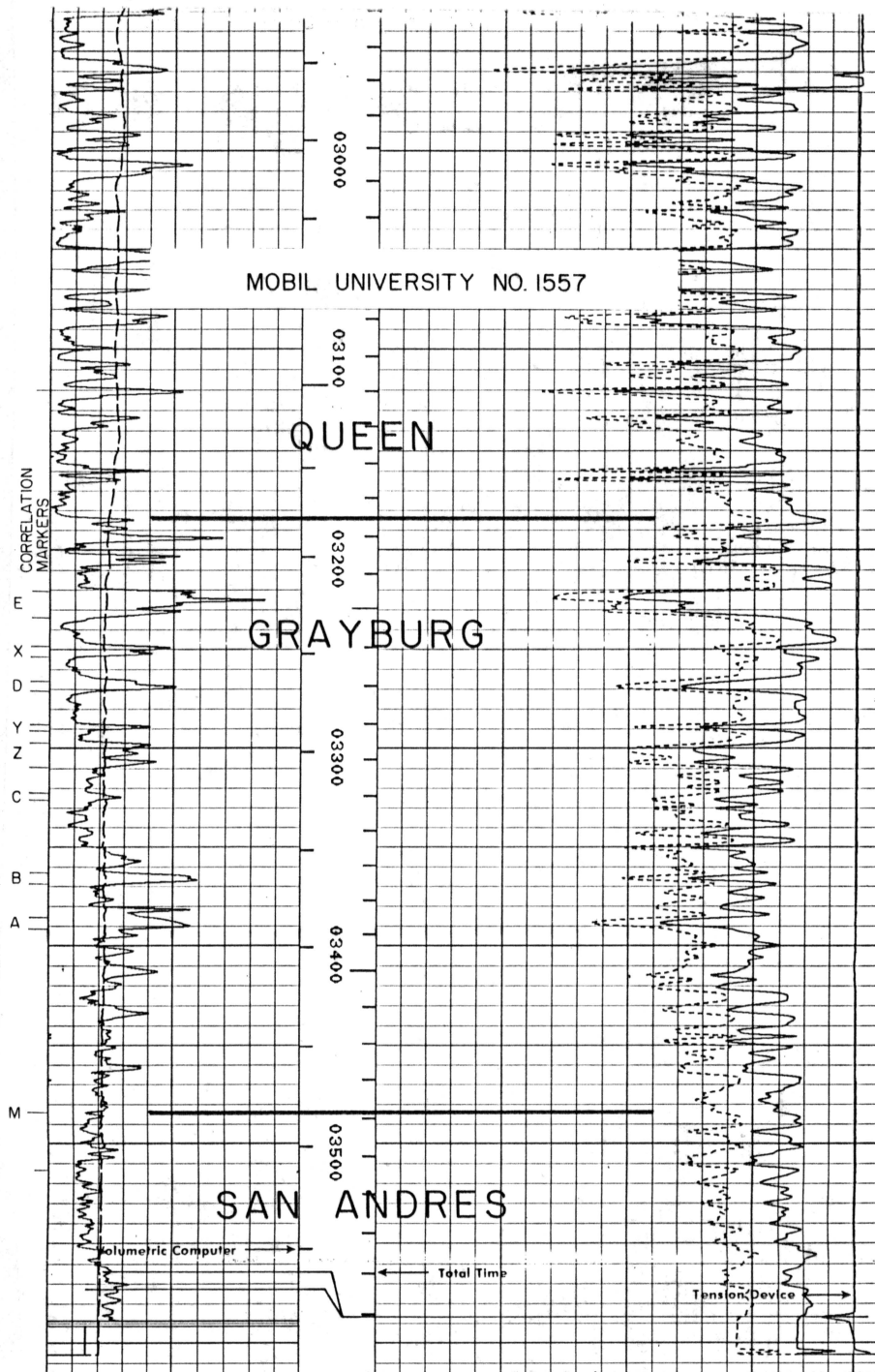


Figure 15. Gamma ray/sonic log of the San Andres, Grayburg, and Queen section in the Mobil University No. 1557.

It is reasonable to expect that these well log and lithologic changes used to pick the Queen, Grayburg, and San Andres should change position in a short distance along the dip direction, reflecting the progradational nature of the overall depositional setting; on the other hand, these contacts should be recognizable for a significant distance in the strike direction, particularly within the same fault block. Because these contacts are not tied to precise geological time and the position of major facies changes such as used here shift depending on position on the platform, these well log and lithologic contacts are expected to vary considerably depending upon the field and the operator. A method of unifying correlations across the platform and from field to field is needed before controls on porosity development can be determined.

The key to conducting detailed studies within the Dune Field has been the correlation of siltstone beds that vary in thickness from 5 to 15 feet; these siltstones are labeled on Figure 15 as A, B, C, Z, Y, D, X, and E, from bottom to top. Siltstones are readily recognized by the high gamma-ray recording, although it is important to note that there are also several high gamma-ray peaks that are not siltstone. The siltstone correlation grid was established by means of a number of closely spaced cross sections (Fig. 16). The thin, widespread nature of the units along with the angular silt-sized particles suggests transportation by wind; the common burrowing suggests that they accumulated mainly in shallow marine and marginal marine environments. Thus, at least in this limited area these siltstone beds represent geological time lines and form the basis for the facies interpretations that follow. Some of the siltstones were probably entirely reworked into local channels or bars and do not even extend completely over the small study area.

In general, the relatively clean siltstone beds record very low permeability and are barriers to vertical movement of fluids. In zones where burrow reworking is intensive, silt

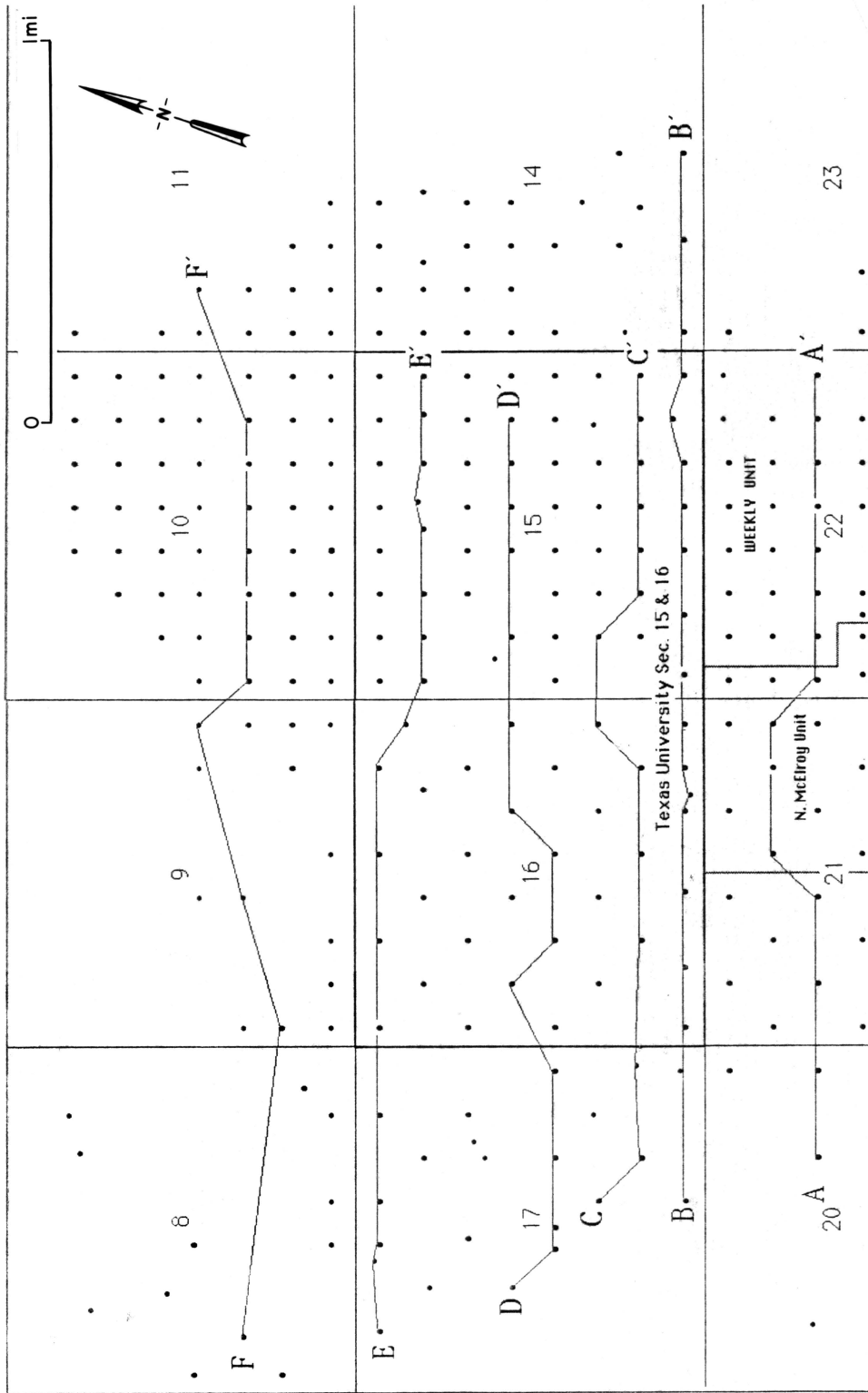


Figure 16. Index map of the study area showing the location of the log correlation cross sections.

may make up as little as 20 percent of the dominantly dolomite rock; these zones do maintain some permeability and cannot be vertical barriers to flow. However, this small percentage of silt is still adequate to cause a typically higher radioactive peak on the gamma-ray log.

## DOLOMITE FACIES

### Introduction

Effective reservoir definition is based on detailed core descriptions through the reservoir section. In this study, slabbed cores were logged on a graphic logging form in order to ensure efficient and standardized recording. The properties visually logged from the slabbed surface, thin sections, and X-ray diffraction are then readily calibrated to the various geophysical logs, core analyses, and log cross plots. The flat surfaces were dry sanded in order to enhance grain and matrix definition.

Because of the extensive dolomitization, many of the original textures and structures have been destroyed or are at least very obscure. Therefore, a certain level of interpretive logging has been necessary with these cores.

### Facies Descriptions

Continuous cores from the nine wells identified earlier were logged in detail. The resultant data were then integrated into more general facies that are described and illustrated in this section.

FACIES NAME: Pisolite (Fig. 17)

LITHOLOGY: Dolomite, anhydrite

COLOR: Variable, but usually very light brown (tan) to medium brown; occasional red silt infill, light pink staining

TEXTURE: Variable within the facies tract from finely crystalline laminated mudstones to pisolite grainstones or packstones

GRAINS:  
 Diagnostic: pisolites  
 Dominant: pisolites, coated grains  
 Present: mollusks, intraclasts

STRUCTURES: Fenestral "birdseye" pores (usually anhydrite cemented), tepee structures, vadose (?) crusts, and sheet cracks occur in the more "evaporitic" facies. Poorly developed parallel laminations in mudstones and grainstones and rare burrows occur throughout the pisolitic facies. Some pisolites show polygonal fitting and inverse grading (interpreted to indicate in situ formation) as well as features consistent with an origin as independent grains. Crinkly (algal?) laminations occur in mudstones interbedded with the pisolites.

THICKNESS: Up to 40 feet

POROSITY RANGE: Very low (up to 5 percent) due to massive cementation by anhydrite

POROSITY TYPE: Not logged

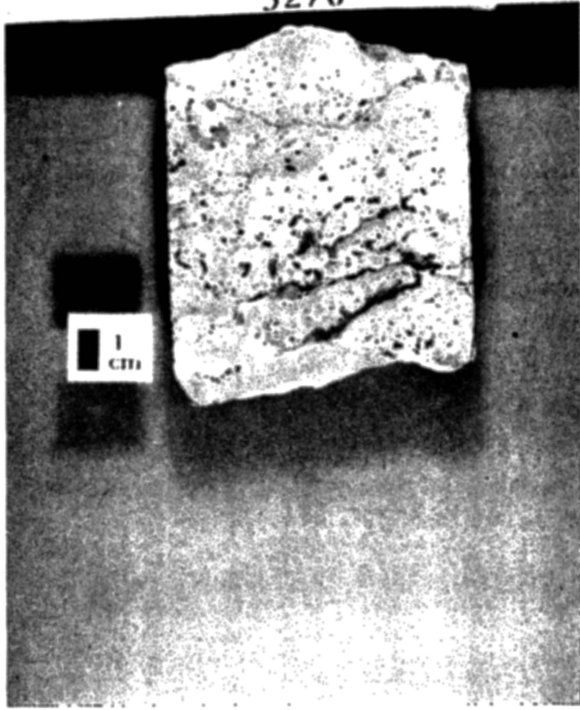
DIAGENESIS: Dolomite crystal size in this facies is generally very small (<20 $\mu$ ), interpreted to indicate early dolomitization. Extensive cementation by calcium sulfate (now anhydrite) occludes most primary pores. Sulfate occurs predominantly as cements in vertical and horizontal cracks and fractures. Nodular textures appear to be less important volumetrically.

OCCURRENCE: Cores from the Mobil University "GG"#4, "CC"#3, #1540

ASSOCIATED FACIES: Ooid grainstone, siltstones, crinkly laminated mudstones

DEPOSITIONAL ENVIRONMENT: Tidal flats on islands of limited areal extent

MOBIL UNIVERSITY 1539  
PISOLITE GRAINSTONE  
3270'

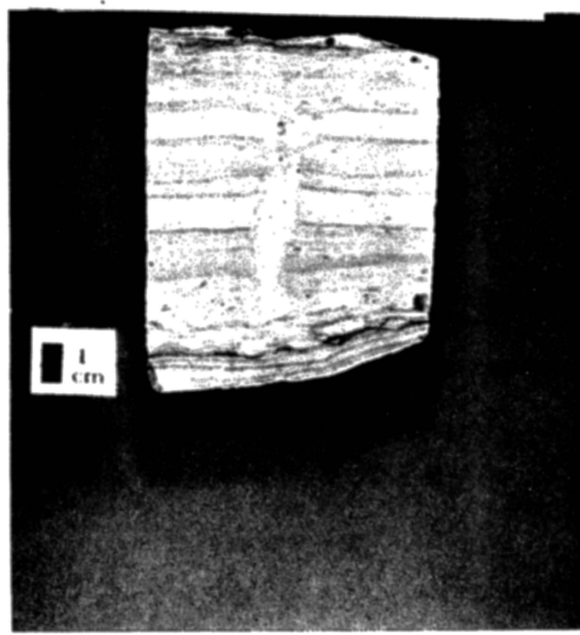


a



b

MOBIL UNIVERSITY 66-1  
LAMINATED MUDSTONE  
3126'



c

MOBIL UNIVERSITY 66-1  
ALGAL LAMINATED  
MUDSTONE  
3075'



d

Figure 17. Pisolite grainstone facies comprising pisolite grainstone (a, b), laminated mudstone (c), and algal laminated mudstone (d) facies. Slabbed surfaces.

**FACIES NAME:** Ooid grainstone (Fig. 18a, b)  
**LITHOLOGY:** Dolomite with anhydrite cement  
**COLOR:** Light brown to medium brown; medium gray to dark gray  
**TEXTURE:** Grainstone; rarely interbedded with wackestones  
**GRAINS:** Diagnostic: Ooids  
 Dominant: Ooids  
 Present: Pellets, coated grains, unidentifiable grains, mollusks, dasycladacean green algae, intraclasts  
**STRUCTURES:** Parallel laminations, crossbedding, wispy laminations, stylolites, burrows, some keystone structures  
**THICKNESS:** 10 to 30 feet  
**POROSITY RANGE:** Up to 5 percent (generally very tight because of anhydrite cement)  
**POROSITY TYPE:** Interparticle, vuggy, moldic  
**OCCURRENCE:** Cores from Mobil University #1535, #1539, #1540, #1625, "CC" #3  
**ASSOCIATED FACIES:** Pellet grainstone, siltstone, pisolite, mollusk wackestone, and mollusk-rich ooid grainstone  
**DEPOSITIONAL ENVIRONMENT:** High-energy shoals adjacent to pisolite islands and offshore bars on basinward side of pellet flats

**FACIES NAME:** Pellet grainstone (Fig. 18c, d)  
**LITHOLOGY:** Dolomite with anhydrite and gypsum cement  
**COLOR:** Medium to dark brown  
**TEXTURE:** Grainstone  
**GRAINS:** Diagnostic: pellets  
 Dominant: unidentifiable  
 Present: pellets, unidentifiable grains, intraclasts  
**STRUCTURES:** Burrows, parallel laminations, stylolites, anhydrite nodules, crystallotopic anhydrite  
**THICKNESS:** 50 to 20 feet  
**POROSITY RANGE:** 5 to 20 percent (generally high)  
**POROSITY TYPE:** Interparticle, moldic, vuggy (mini-vugs concentrated between grains)  
**OCCURRENCE:** Cores from the Mobil University #1535, #1539, #1540; Gulf State "EE" #7; Getty North McElroy Unit #2217  
**ASSOCIATED FACIES:** Fusulinid wackestone, ooid grainstone  
**DEPOSITIONAL ENVIRONMENT:** Very shallow water burrow flat (possibly partially exposed at low tide)

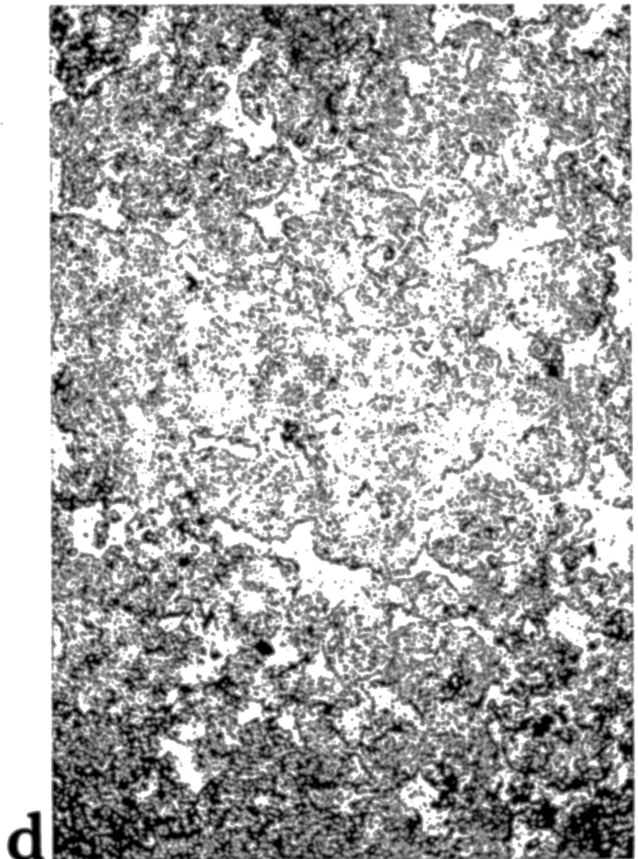
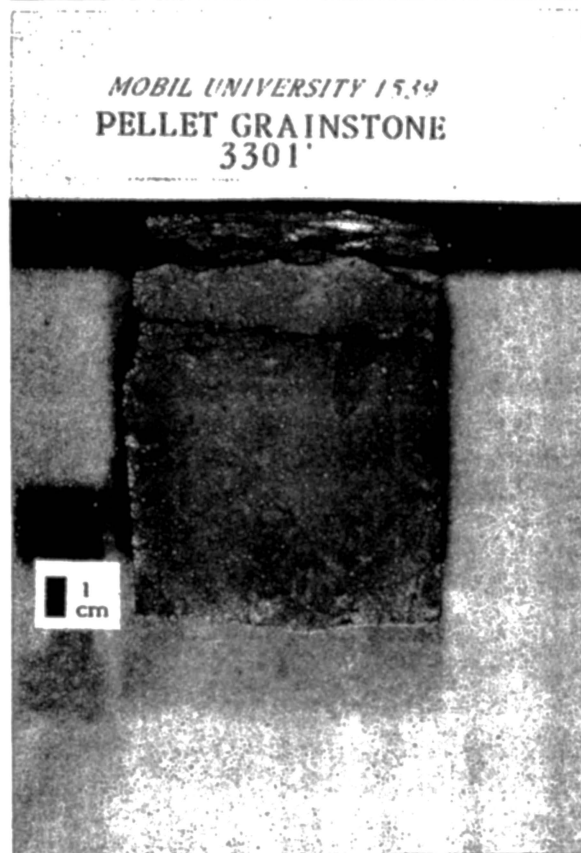
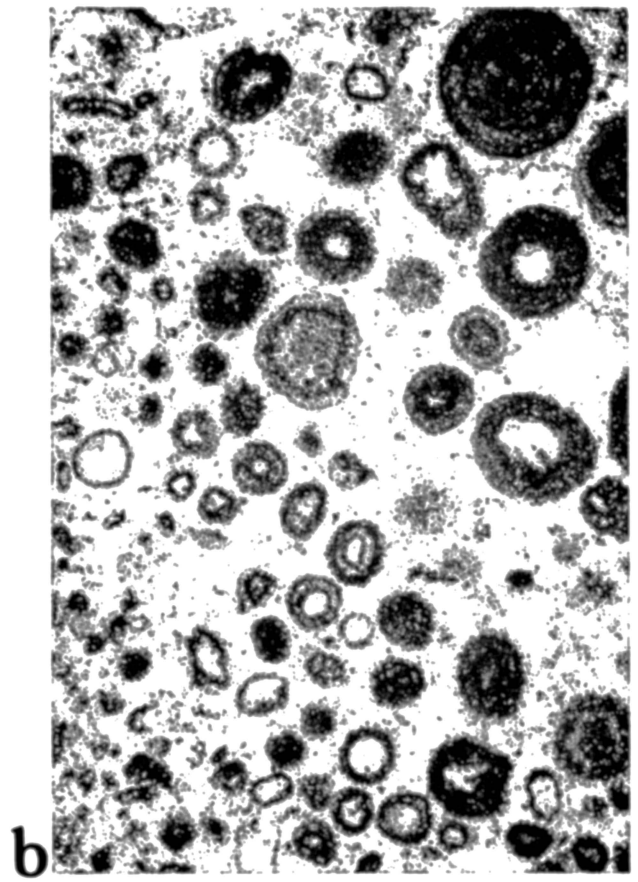
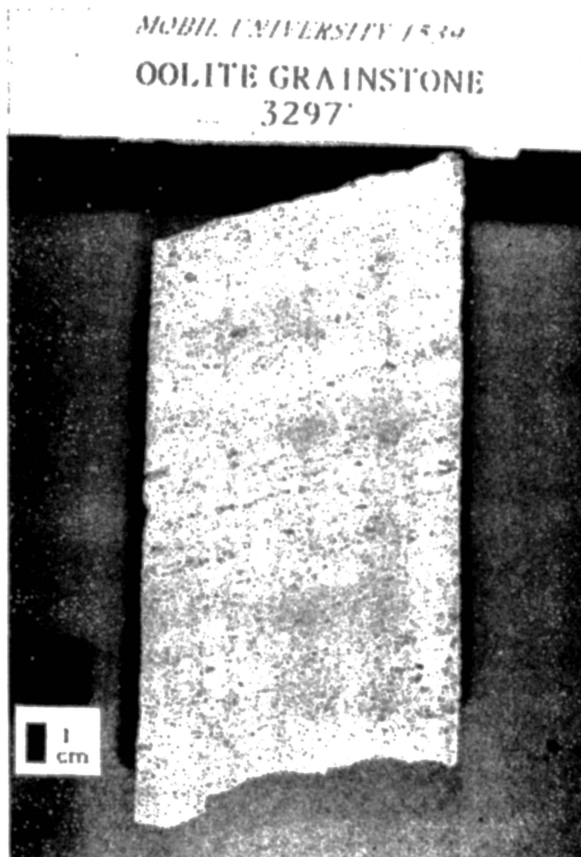


Figure 18. Ooid and pellet grainstone facies.

- a. Crossbedded ooid grainstone. Slabbed surface.
- b. Ooid grainstone. Thin section, X20, from Mobil University No. CC3, 3,139 feet.
- c. Burrowed pellet grainstone. Slabbed surface.
- d. Pellet grainstone. Thin section, X20, from Mobil University No. 1539, 3,337 feet.

FACIES NAME: Fusulinid wackestone (Fig. 19)

LITHOLOGY: Dolomite with anhydrite and gypsum cement

COLOR: Light brown to medium brown to dark brown; light gray; grayish brown; mottled colors common, perhaps being porosity-specific (medium brown color appears more altered, with higher matrix porosity)

TEXTURE: Wackestone (common), packstone (rare)

GRAINS: Diagnostic: fusulinids  
Dominant: fusulinids  
Present: gastropods, pelecypods, crinoids, bryozoans, green algae

STRUCTURES: Wispy laminations, stylolites, burrows, compaction-aligned fusulinids, geopetal structures, vertical fractures (cemented with anhydrite), anhydrite nodules

THICKNESS: Up to 150 feet

POROSITY RANGE: Up to 10 percent, occasionally higher

POROSITY TYPE: Intercrystalline (matrix), moldic (after leached fusulinids), vuggy porosity when total porosity is higher; intraparticle when fusulinid skeletal structure is preserved.

DIAGENESIS: Fusulinids exhibit range of preservation from completely leached and filled with anhydrite cement to total preservation; total preservation is rare, perhaps controlled by micritization in shallower (?) waters. The greatest volume of porosity is in the form of intercrystalline matrix to vuggy porosity. Dolomite crystal sizes range upward to about 60 $\mu$  in diameter.

OCCURRENCE: Cores from the Mobil University #1532, #1535, #1539, #1540, #1625; Gulf Oil "EE" #7, "EB" #9

ASSOCIATED FACIES: Crinoid-bryozoan, pellet packstone, sponge-algal framestone, ooid (?)/pellet grainstone, siltstone

DEPOSITIONAL ENVIRONMENT: Shallow-water platform or shelf, probably with widely varying water depths

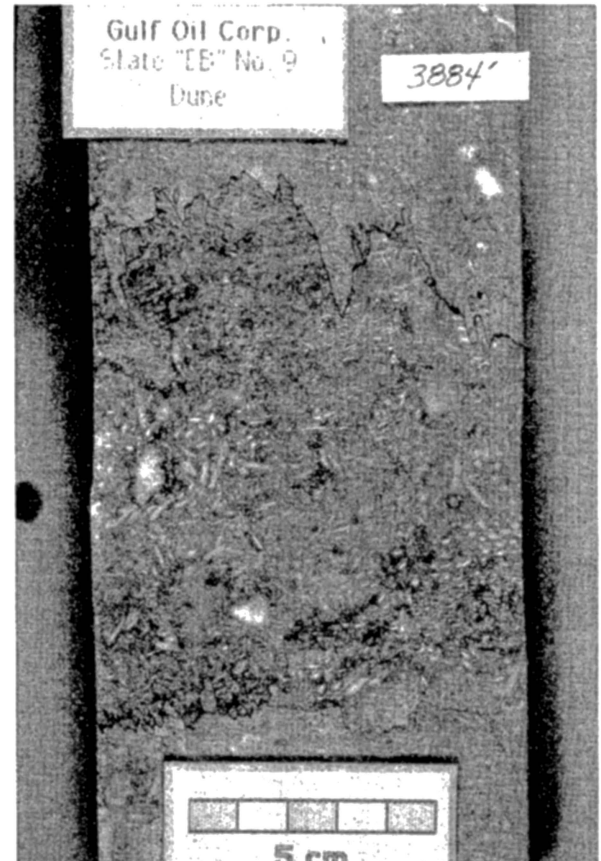
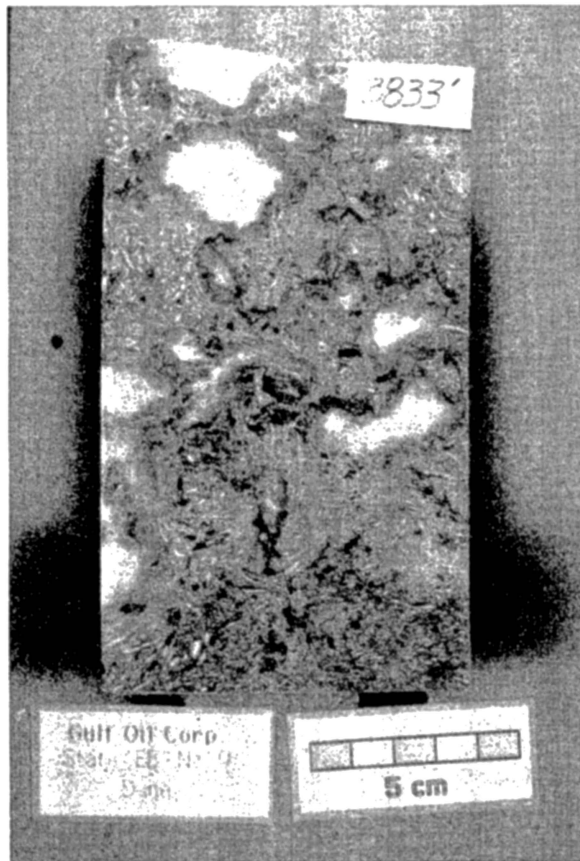
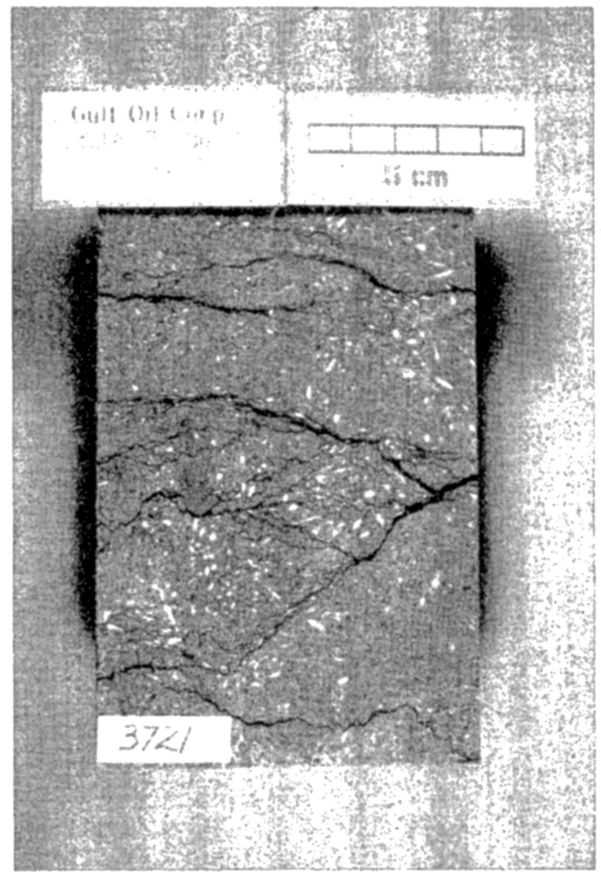
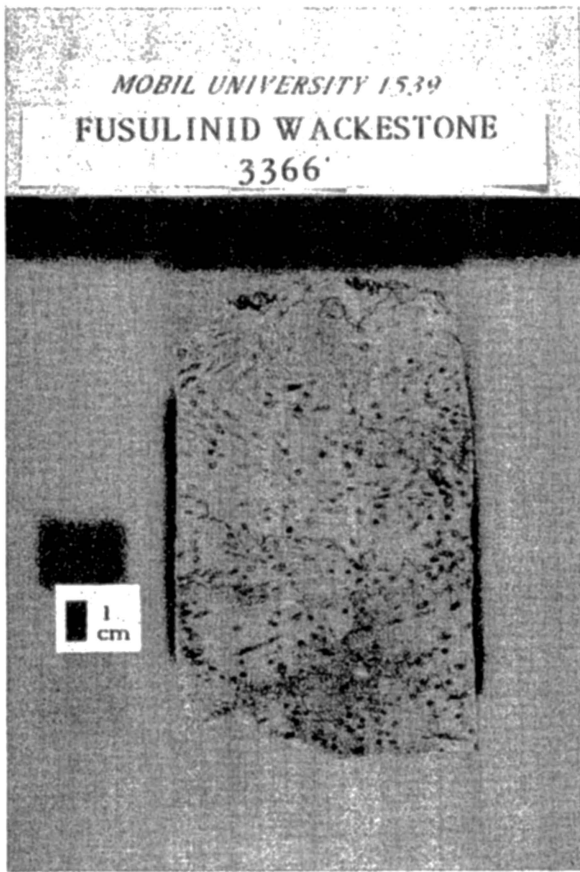


Figure 19. Fusulinid wackestone facies.

FACIES NAME: Sponge-algal framestone (Fig. 20)

LITHOLOGY: Dolomite with anhydrite and gypsum cement

COLOR: Light gray to medium brown to dark brown (mottled)

TEXTURE: Wackestone and framestone

GRAINS: Diagnostic: growth structures  
Dominant: fusulinids, mollusks  
Present: crinoids, bryozoans, mollusks

STRUCTURES: Vertically aligned structures with sharp to diffuse boundaries. The structures are from a few to several centimeters wide, reach 20 to 30 centimeters in length, and are usually cylindrical to oblate in three dimensions. Across the boundary of the structures there is usually a difference in color, dolomite crystal size, fusulinid packing and orientation (when fusulinids are present), mold content, and anhydrite content. Very rarely structures attributed to sponge pore systems are preserved at the edges of these structures, but others seem to have faint laminations (algal?). Burrows, brecciation, fractures, stylolites, aligned fusulinids, and massive and nodular anhydrite are also common.

THICKNESS: 5 to 70 feet

POROSITY RANGE: Up to 15 percent

POROSITY TYPE: Moldic, vuggy, and intercrystalline

OCCURRENCE: Mobil University #1625, "CC"#3, "GG"#4

ASSOCIATED FACIES: Fusulinid wackestone, siltstone, crinoid-bryozoan-pellet

DEPOSITIONAL ENVIRONMENT: Possibly low-energy shelf edge developed on a very low gradient slope

DISCUSSION: Poor preservation generally prohibited positive identification of sponge types, but they probably were calcareous sponges, as based on overall shape. The "sponge" structure usually has darker color, smaller dolomite crystals, and a higher percentage of moldic porosity than the surrounding rock. The "country" rock usually is a skeletal wackestone of low biotic diversity with intercrystalline and moldic porosity sometimes plugged with anhydrite. The structures observed are more suggestive of the Guadalupian Goat Seep Reef described by Crawford (1981) or the algal-sponge-brachiopod mounds of the Lower Permian (Wolfcamp age) Laborcita bioherms described by Toomey and Cys (1979) than the oft-cited sponge-algal boundstone of the Upper Permian Capitan Formation (Babcock, 1977; Yurewicz, 1977).

This poorly preserved, muddy facies, rich in sponges and algae is thought to be the same as Longacre's "exposed flat" facies (Longacre, 1980, 1983), and has characteristics similar to, but not as well developed as, the reef facies in the North McElroy Field (Longacre, 1980). Longacre's description of the exposed flat facies is not unlike the mud-rich framestone facies. Longacre described the exposed flat facies as a "low complex of mounds out on the shallow shelf or in a belt along the coast" (Longacre, 1980, p. 112).

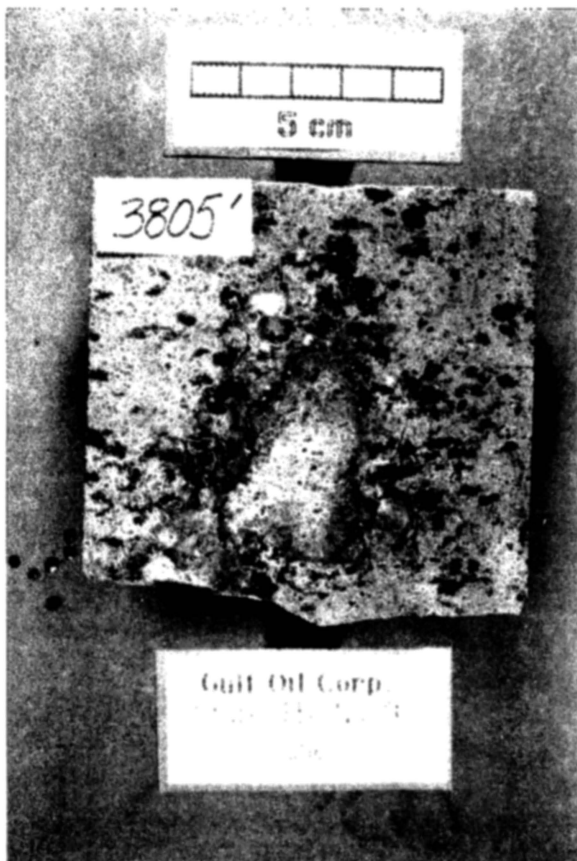
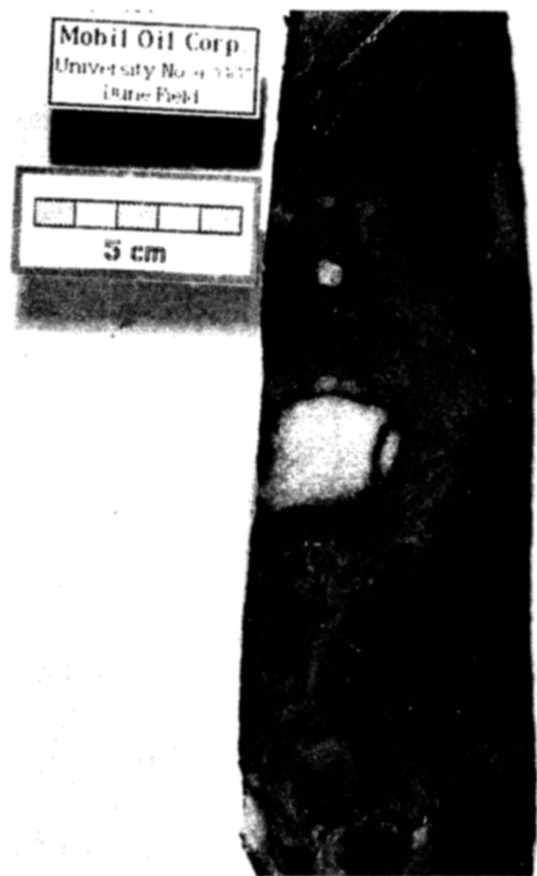


Figure 20. Sponge-algal framestone facies.

FACIES NAME: Siltstone (Fig. 21)

LITHOLOGY: Quartz with dolomite, disseminated pyrite, and anhydrite cement

COLOR: Medium to dark gray, medium brown

TEXTURE: Quartz-rich siltstones and fine sandstones; silty and sandy dolomitic mudstones to grainstones

GRAINS: Diagnostic: terrigenous silt and fine sand  
 Dominant: usually terrigenous silt and fine sand, although this can be a smaller fraction of a dolomitic silt  
 Present: unidentifiable grains, intraclasts, coated grains, pellets, mollusks

STRUCTURES: Abundant burrows, wispy laminations, minor crossbedding (commonly associated with admixed sand-sized carbonate grains), stylolites, crystallotopic anhydrite

THICKNESS: 3 to 30 feet

POROSITY RANGE: Up to 5 percent

POROSITY TYPE: Interparticle

OCCURRENCE: Cores from the Mobil University "GG"#4, "CC"#3, #1535, #1540, #1539, #1625; Gulf State "EB"#9, "EE"#7; Getty North McElroy Unit #2217

ASSOCIATED FACIES: Pisolite, fusulinid wackestone, pellet grainstone, mollusk wackestone, ooid, mud-rich framestone (1625)

DEPOSITIONAL ENVIRONMENT: Transported by wind; deposited and reworked in all environments, but best preserved in lower-energy settings

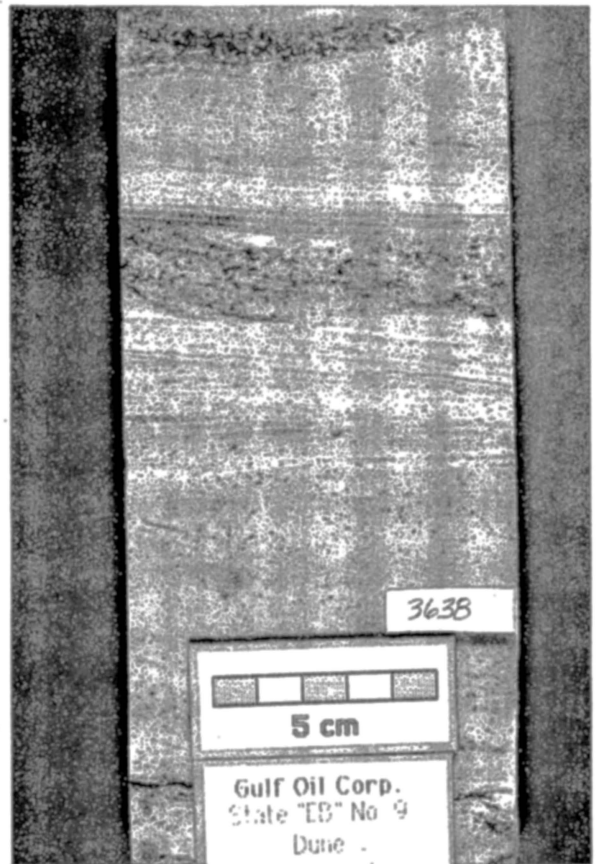
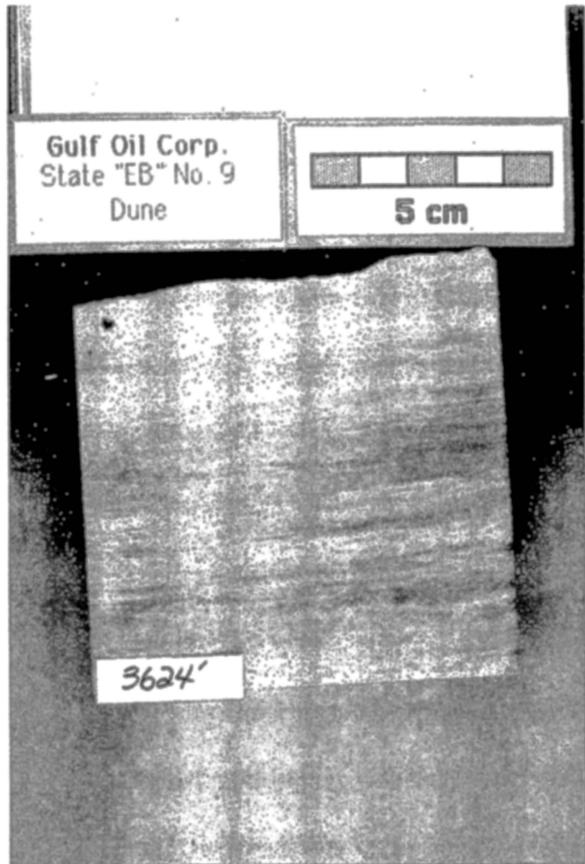
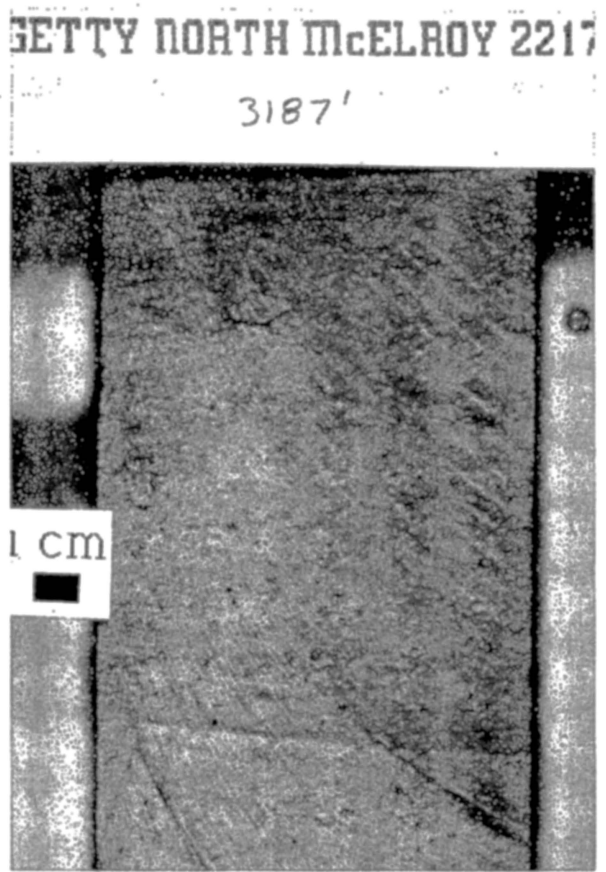
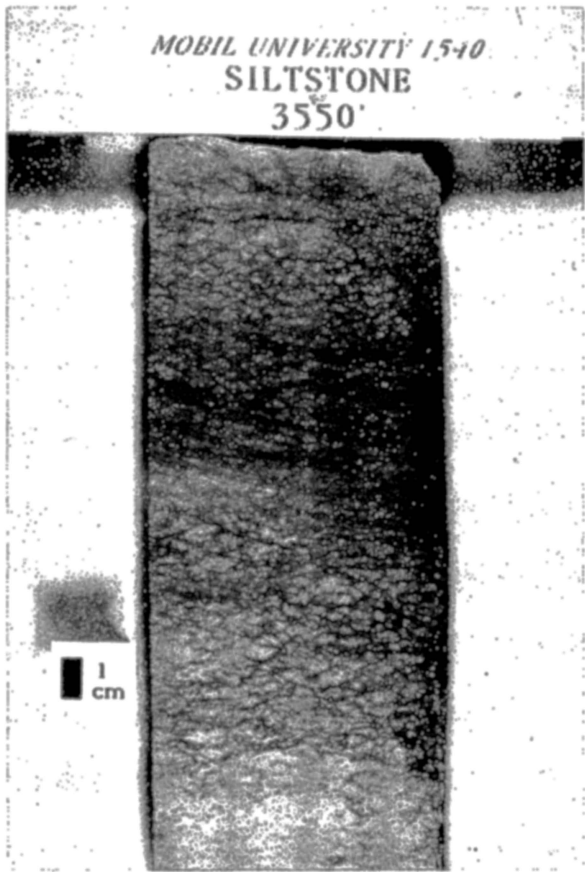


Figure 21. Siltstone facies.

**FACIES NAME:** Crinoid-bryozoan-pellet facies

**LITHOLOGY:** Dolomite with anhydrite and gypsum cement

**COLOR:** Light brown to medium brown; light gray to medium gray

**TEXTURE:** Packstone; common grainstone and wackestone; some framestone

**GRAINS:**  
 Diagnostic: crinoids, sponges, bryozoans  
 Dominant: pellets, unidentifiable grains, fine skeletal debris  
 Present: mollusks, bryozoans, crinoids

**STRUCTURES:** Growth structures, stylolites, crystallographic and nodular anhydrite. Distinct lack of bedding, although beds of the two subfacies are distinctly interbedded.

**DISCUSSION:** Two subfacies are characterized by different grain types. The crinoid-bryozoan packstone subfacies is generally light to medium gray in color and shows very loose packing of allochems. Growth structures with well-preserved sponge skeletal structure occur in this subfacies. The allochems are crinoids, bryozoans, and sponge fragments in a very fine matrix of unidentifiable grains and mud. Primary porosity is occluded by anhydrite cement. The crinoid-pellet packstone subfacies is light to medium brown in color, and rich in sand-sized unoxidized pellets. Remains of bryozoans, sponges, and crinoids are scattered throughout, but not nearly as abundant as in the skeletal subfacies. No growth structures were observed in the pellet subfacies. Vuggy porosity appears to be greater in the pellet subfacies than in the skeletal subfacies.

**THICKNESS:** 50 to 80 feet.

**POROSITY RANGE:** Up to 15 percent

**POROSITY TYPE:** Vuggy and moldic

**OCCURRENCE:** Cores from the Mobil University #1539(?), #1535, #1540; Gulf State "EB" #9, "EE" #7; Getty North McElroy Unit #2217(?)

**ASSOCIATED FACIES:** Fusulinid wackestone, sponge-algal framestone

**DEPOSITIONAL ENVIRONMENT:** Shallow-water shelf and slope

## Vertical Facies Distribution

Vertically, the cored section in Unit 15/16 can be subdivided into three parts (Figs. 22 and 23): (1) the lower unit below the M marker, (2) the middle unit between the M and A markers, and (3) the upper unit from the A marker to the base of the "Brown Lime." The lower unit, which occurs beneath the production zone, comprises fusulinid wackestone in all wells studied. This lower fusulinid wackestone reaches a total thickness of 140 feet in the Getty 2217, the only well to penetrate it completely. It is assumed that shoal-water equivalents of these shelf carbonates occur platformward of the Unit 15/16. The fusulinid wackestone in the lower unit typically has very low matrix porosity, and the fusulinids are preserved as molds (porosity) or molds filled with anhydrite and gypsum. The difference in facies and diagenetic patterns from those of the overlying reservoir section suggests that a major geological break exists at the M marker, at the top of the lower unit. In addition, the gamma-ray curve shows a pronounced low-gamma shoulder at the M marker and provides ready correlation throughout the area. For these reasons, this horizon has been selected as the operational top of the San Andres dolomite.

The middle unit consists of crinoid-bryozoan-pellet facies (interbedded crinoid-bryozoan packstone and crinoid-pellet packstone) across the eastern two-thirds of the area and sponge-algal framestone in the western one-third. This unit extends from the M marker at the base to the A siltstone at the top. The upper unit, which is defined as extending from the A siltstone at the base to the "Brown Lime" at the top, constitutes a single upward-shoaling (progradational) cycle. The vertical sequence consists of fusulinid wackestone at the base, pellet and ooid grainstone near the top, and pisolite grainstone and anhydrite at the top. Several siltstone beds occur throughout the unit; the siltstone beds are thicker and more closely spaced toward the top.

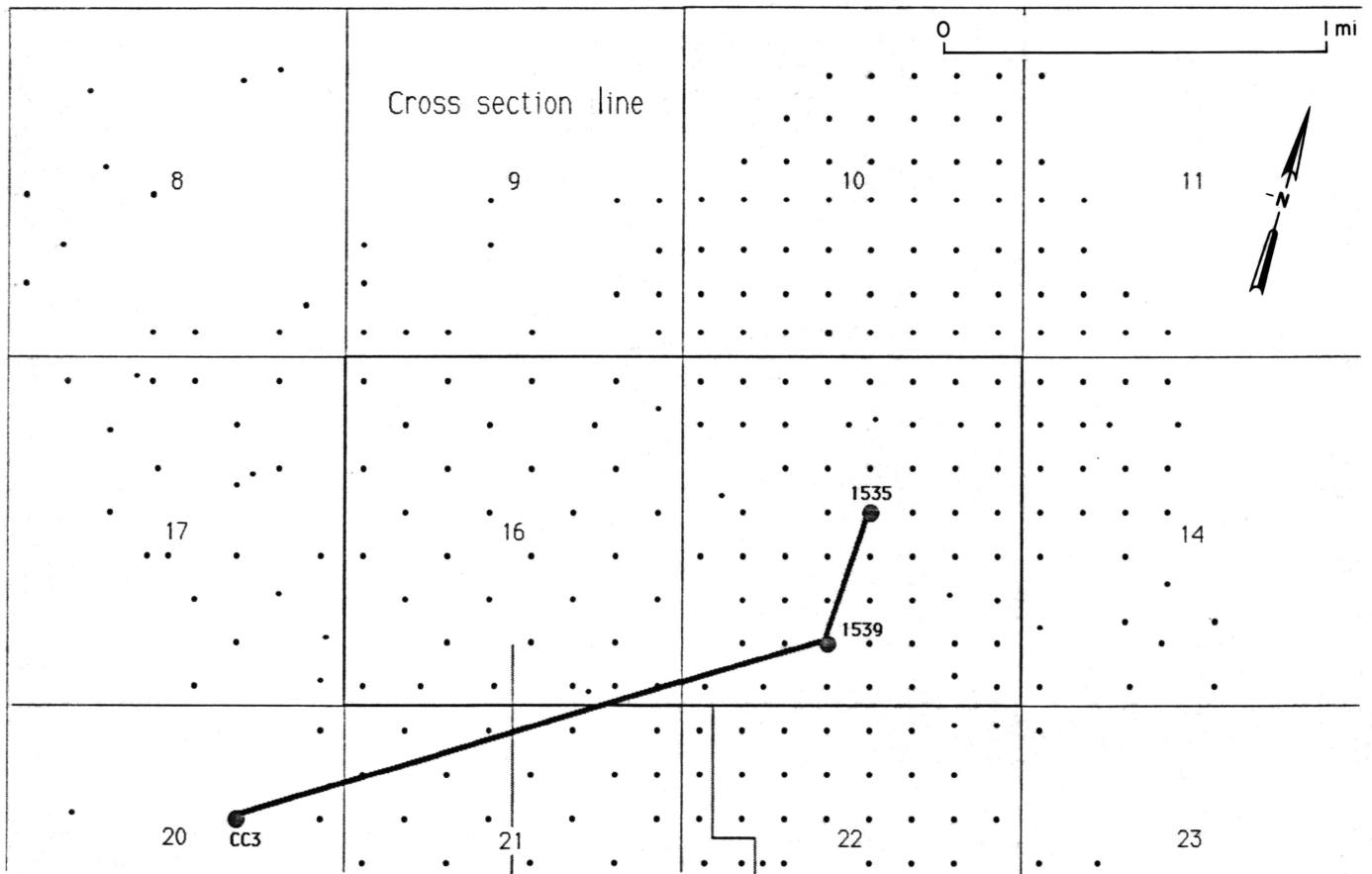


Figure 22. Index map of the study area showing location of the detailed facies cross section.

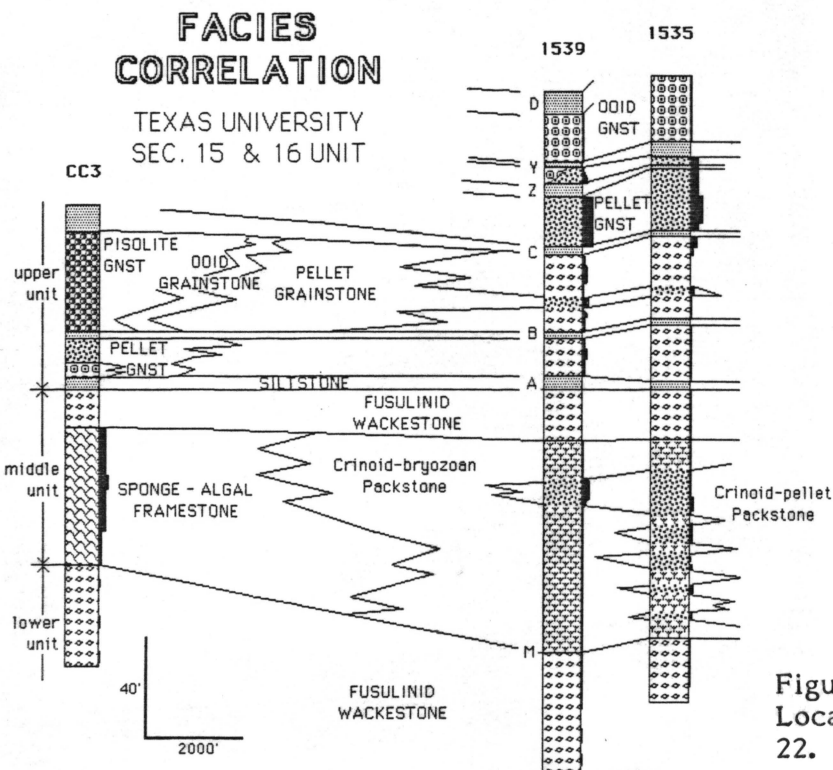


Figure 23. Detailed facies cross section. Location of section is shown on Figure 22.

## Lateral Facies Distribution

The facies descriptions and vertical distribution of facies discussed previously were obtained from detailed study of cores from the nine wells identified earlier. However, assuming that many facies have characteristic log responses, it is also possible to supplement core data with log cross-plot data in constructing facies maps, and thus to aid in determining where facies changes occur between cored wells.

Various cross-plot methods can be effective in aiding identification of carbonate facies, particularly when used in conjunction with other guides such as facies maps and cross sections. However, the key to proper use of these methods is obtaining reliable core data and using the core data to calibrate the logs. Core-calibrated log cross plots used with facies maps and cross sections can be effective in defining where facies changes take place across the field.

Two cross-plots have been made, one for the western area, where only gamma-ray neutron and laterologs are available, and one for the eastern area, where sonic and compensated neutron logs (CNL) are available.

The cross-plot of resistivity from the deep laterolog and neutron porosity (limestone scale) for the western area was constructed using log and rock description data from two cored wells. The results (Fig. 24) show that the siltstone and anhydritic pisolite facies group uniquely and that the framestone and fusulinid wackestone are intermixed. There are too few data points for the ooid and pellet facies to allow us to draw conclusions concerning their distribution. The lack of gypsum in the siltstone and anhydritic pisolite facies suggests that the porosity readings from the neutron log are reasonable. These two facies are not productive; therefore, they can be assumed to indicate the area on the plot that represents 100 percent water saturation. The presence of gypsum in the framestone and fusulinid wackestone makes the porosity values from the neutron unreliable. Therefore, although the higher resistivity for these facies indicates oil saturation, no oil

SEDIMENTARY FACIES CROSS PLOT  
NEUTRON POROSITY VS RESISTIVITY

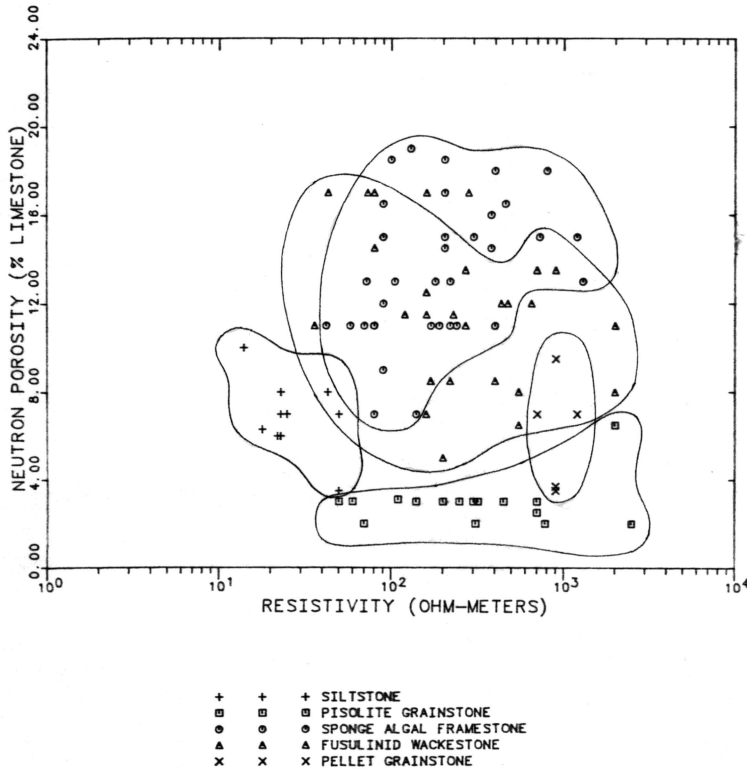


Figure 24. Cross plot of neutron porosity vs. resistivity using wells from the west half of the study area. The various facies as identified from core examination are indicated by the different symbols.

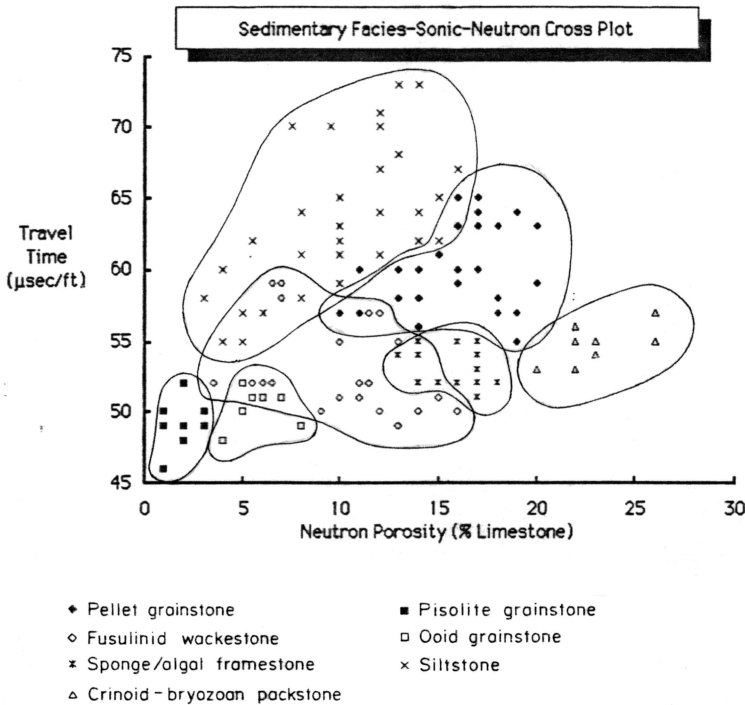


Figure 25. Cross plot of sonic travel time vs. neutron porosity using wells from the east half of the study area. The various facies as identified from core examination are indicated by the different symbols.

saturation calculations can be made. Some of the scatter shown in the Figure 24 plot is due to thin bed and boundary effects.

The cross plot for the eastern area based on sonic and CNL log values together with core description (Fig. 25) shows that, with the exception of the fusulinid wackestone, the facies have fairly distinctive groupings. The siltstone facies plots along a line parallel to the sandstone line but offset toward anhydrite and dolomite, reflecting the admixture of these minerals with the quartz silt. The framestone and crinoid-bryozoan facies plot below the dolomite line, suggesting significant amounts of gypsum. Some data points from the pellet facies plot in this area as well, but most of these points plot between dolomite and anhydrite. The fusulinid wackestone values appear to lie in an intermediate position but are too scattered to be unique.

Facies-distribution maps have been prepared using the various siltstone beds and the M marker as facies boundaries. The section generally penetrated by all wells can be divided into three major units. The lower unit comprises all of the section from the deepest part of the cores up to the M marker. A map of this unit was not prepared because the unit is everywhere represented by fusulinid wackestone, suggesting that it is evenly distributed over the area. A thin grainstone occurs at the top of this lower unit in several of the cores; the contact with the overlying middle unit is sharp.

The middle unit (Fig. 23) extends from the M marker to the A siltstone. The map of this unit (Fig. 26) shows the sponge-algal framestone as a northwest-southeast trend across the western quarter of the area. The middle half of the area comprises the crinoid-bryozoan packstone facies, and the remaining quarter on the east is dominated by the crinoid-pellet packstone, also with a northwest-southeast trend. In general, the entire unit thickens from the western side, where it ranges from 70 to 80 feet thick, to the eastern side, where it is greater than 110 feet thick.

The upper unit consists of a number of dolomites (Figs. 28 through 30, 32, 34, and 35) separated by siltstone beds (Figs. 27, 31, and 33). The siltstone beds, relatively widely

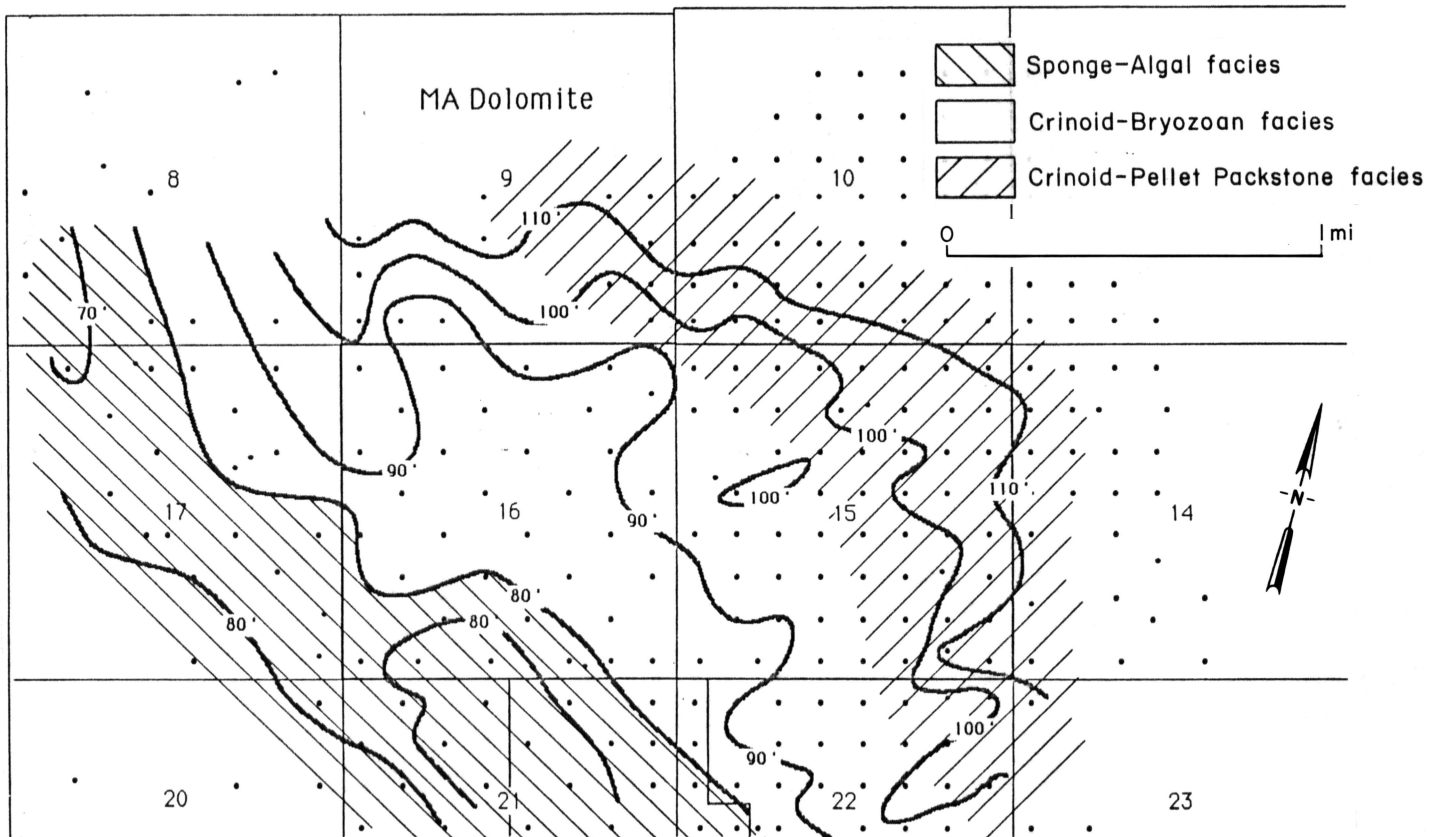


Figure 26. Thickness of the MA Dolomite. The facies represented in this unit are indicated by the hachures.

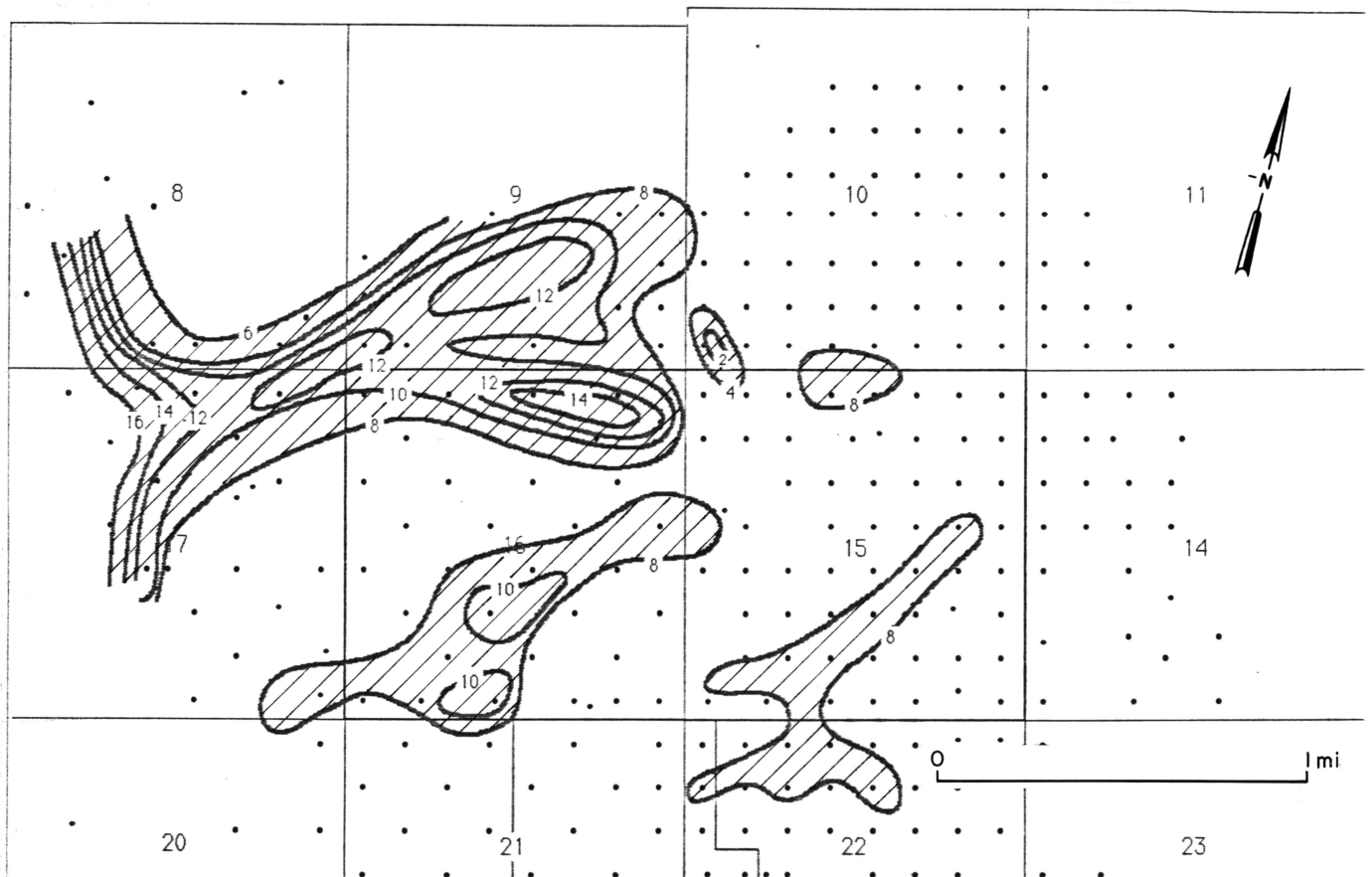


Figure 27. Thickness of the A Siltstone. Although this siltstone extends throughout the study area only the thicker part is indicated by the hachures.

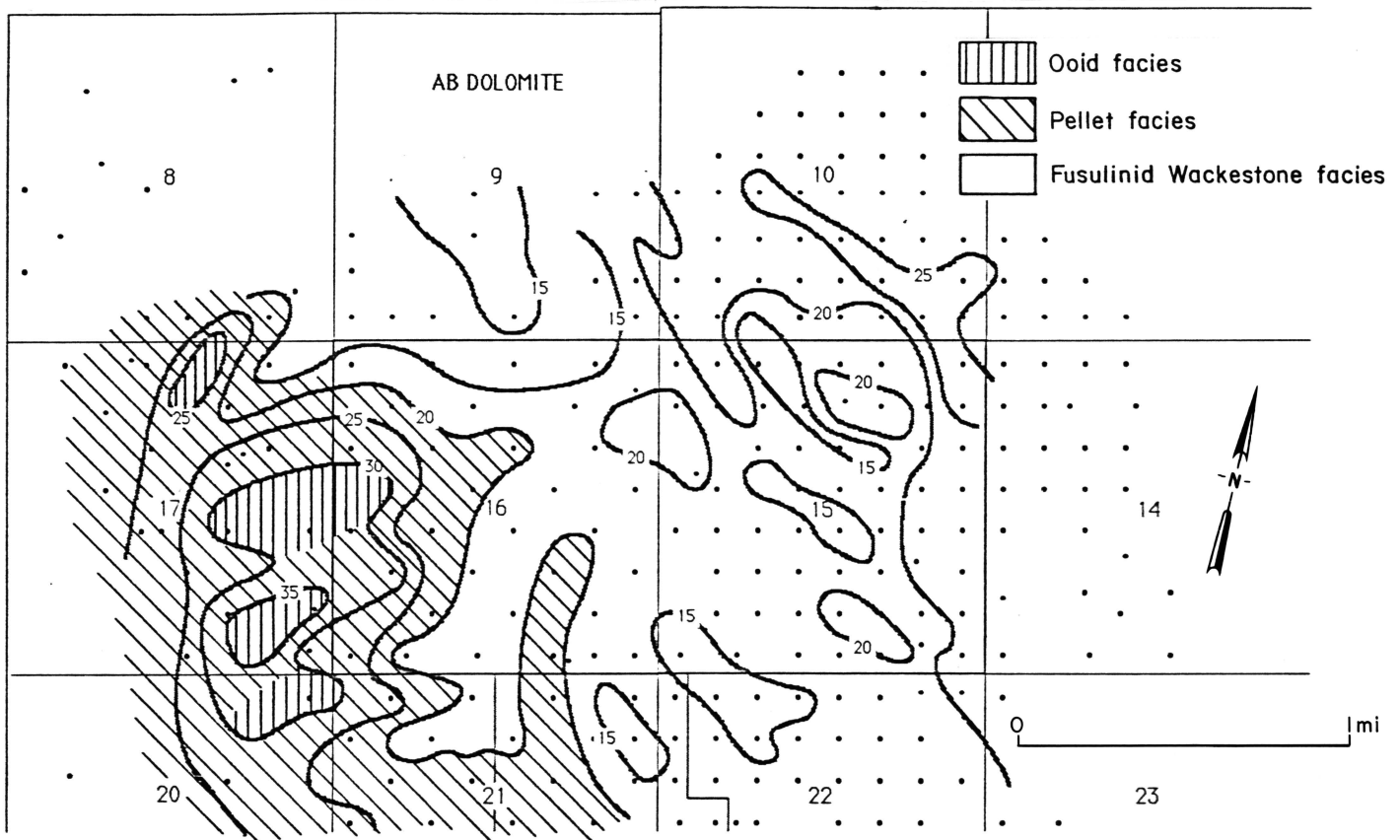


Figure 28. Thickness of the AB Dolomite. The facies represented in this unit are indicated by the hachures.

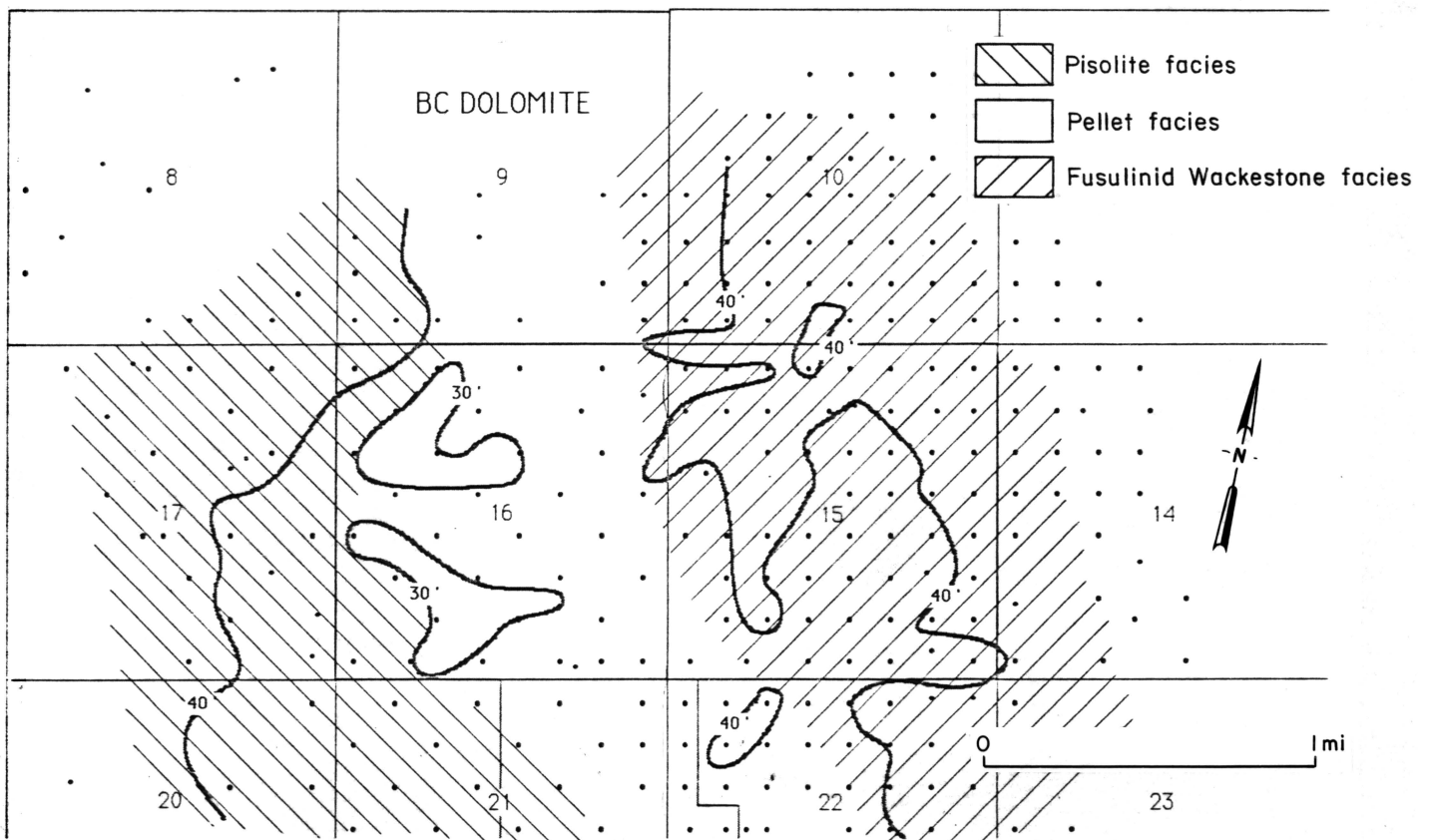


Figure 29. Thickness of the BC Dolomite. The facies represented in this unit are indicated by the hachures.

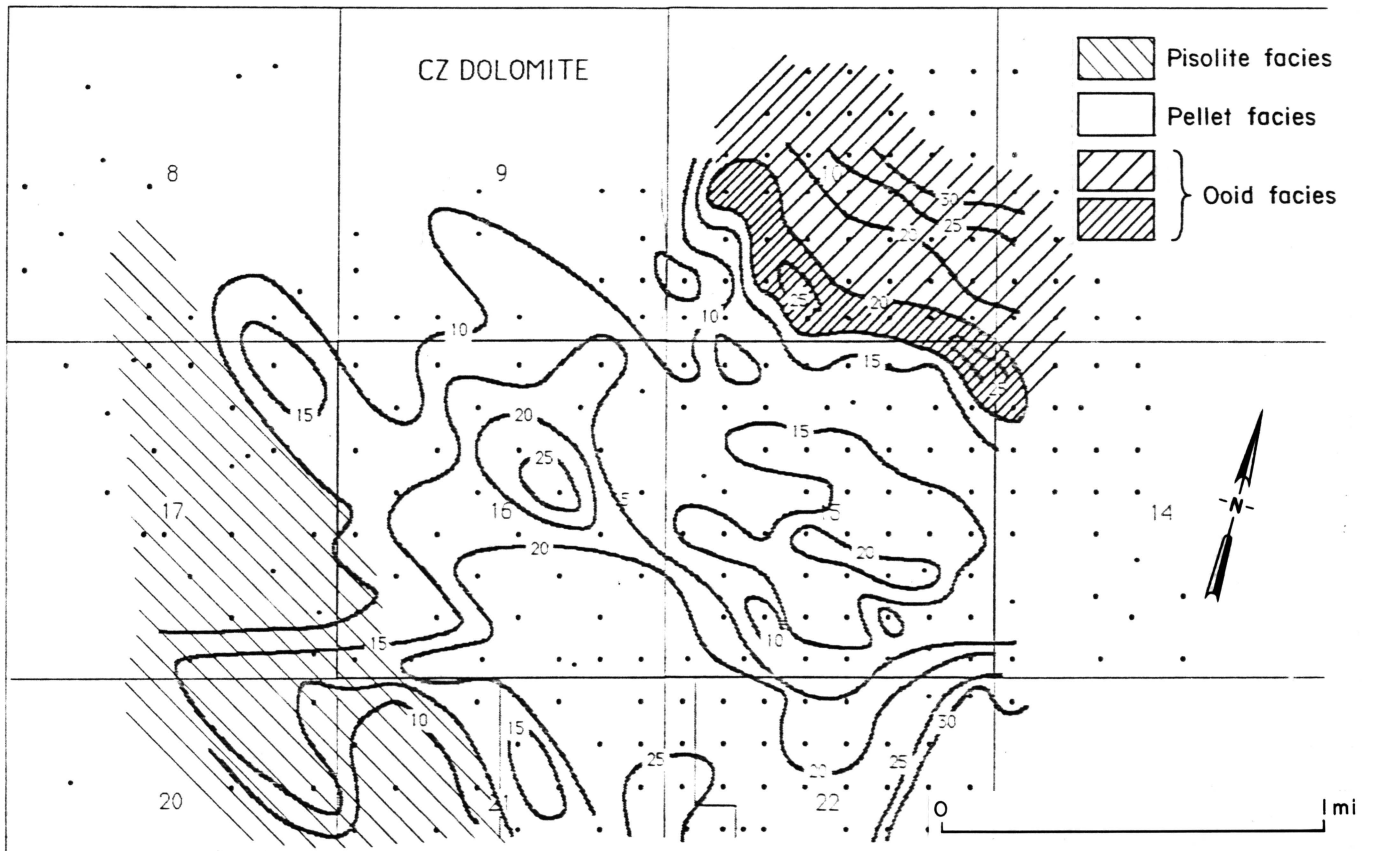


Figure 30. Thickness of the CZ Dolomite. The facies represented in this unit are indicated by the hachures.



Figure 31. Thickness of the Z Siltstone.

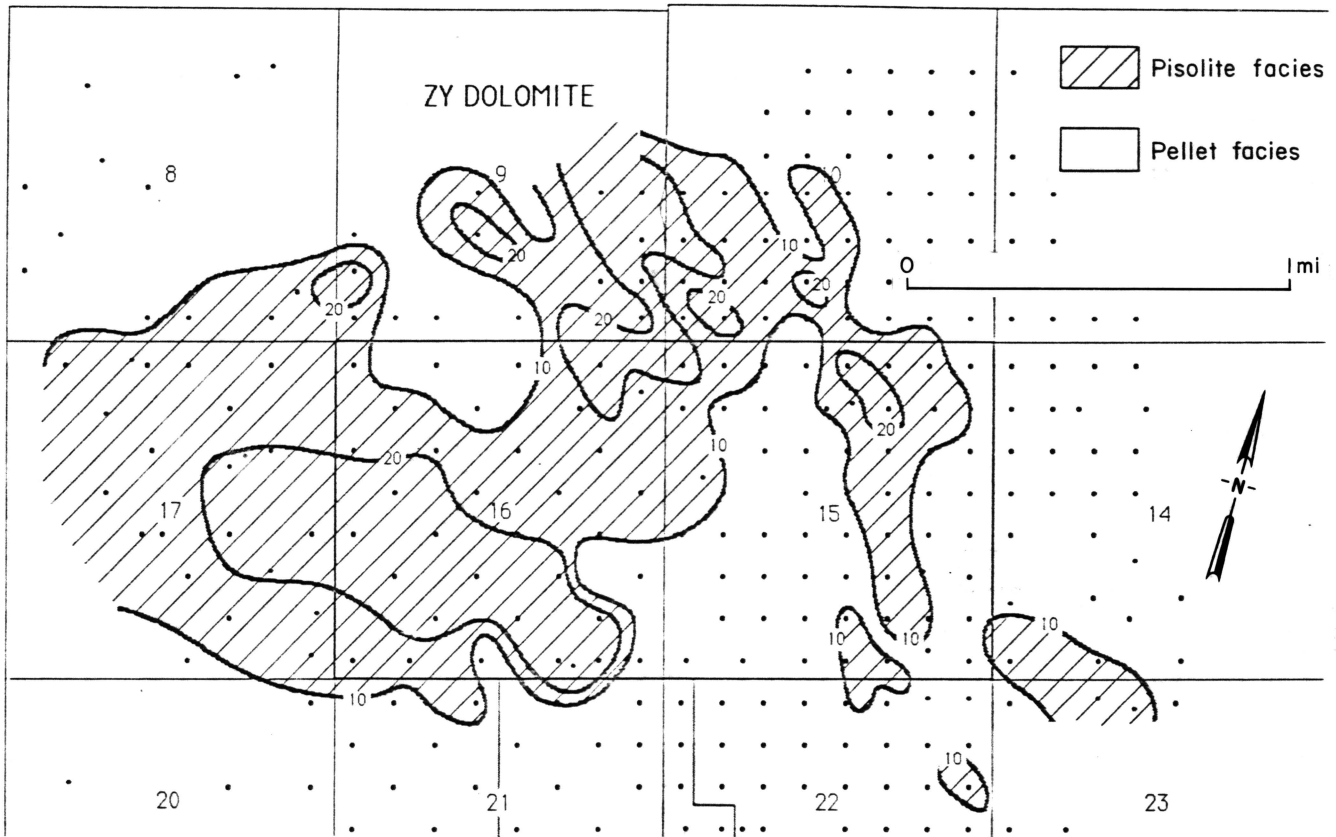


Figure 32. Thickness of the ZY Dolomite. The facies represented in this unit are indicated by the hachures.

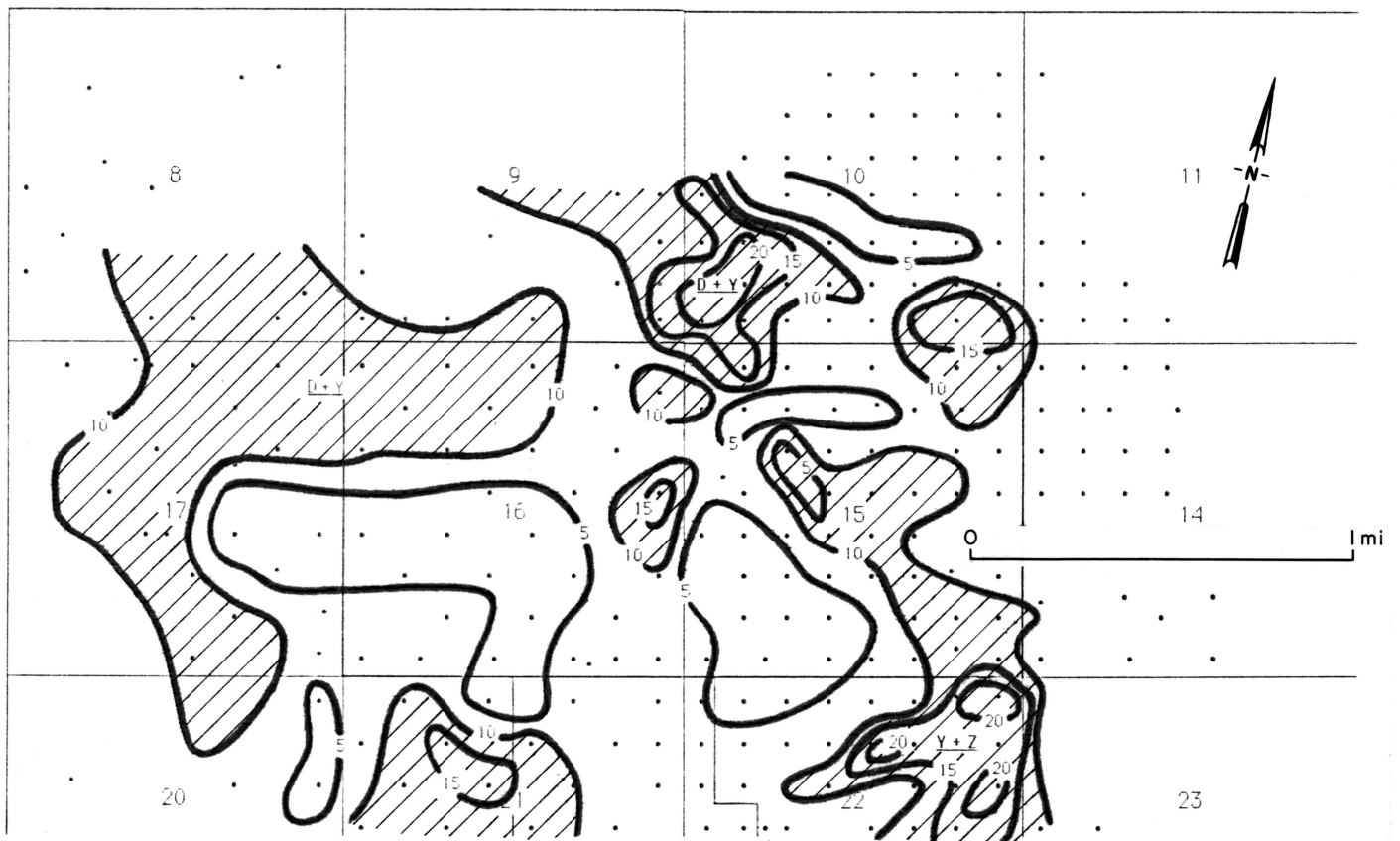


Figure 33. Thickness of the Y Siltstone. The thicker areas are indicated by the hachures.

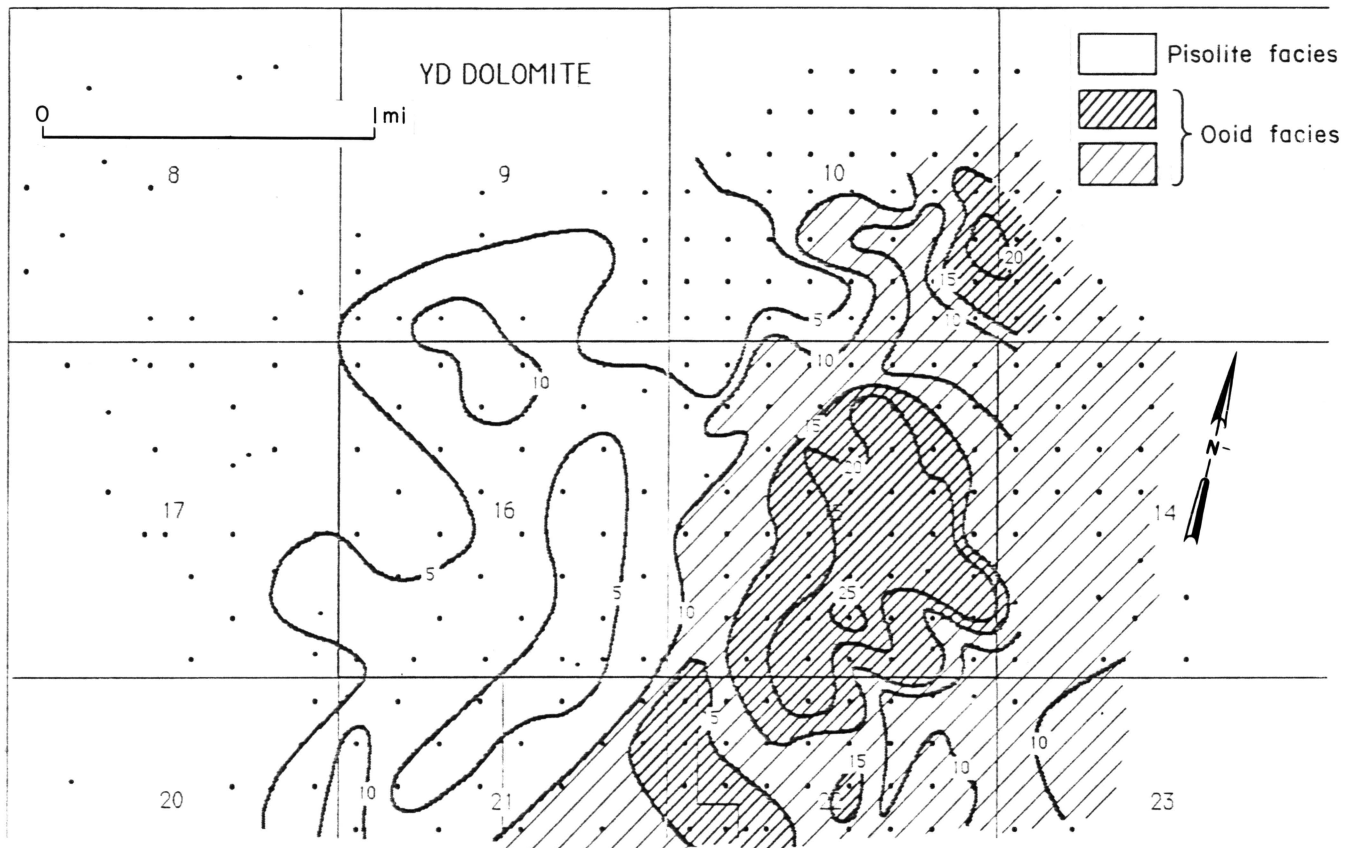


Figure 34. Thickness of the YD Dolomite. The facies represented in this unit are indicated by the hachures.

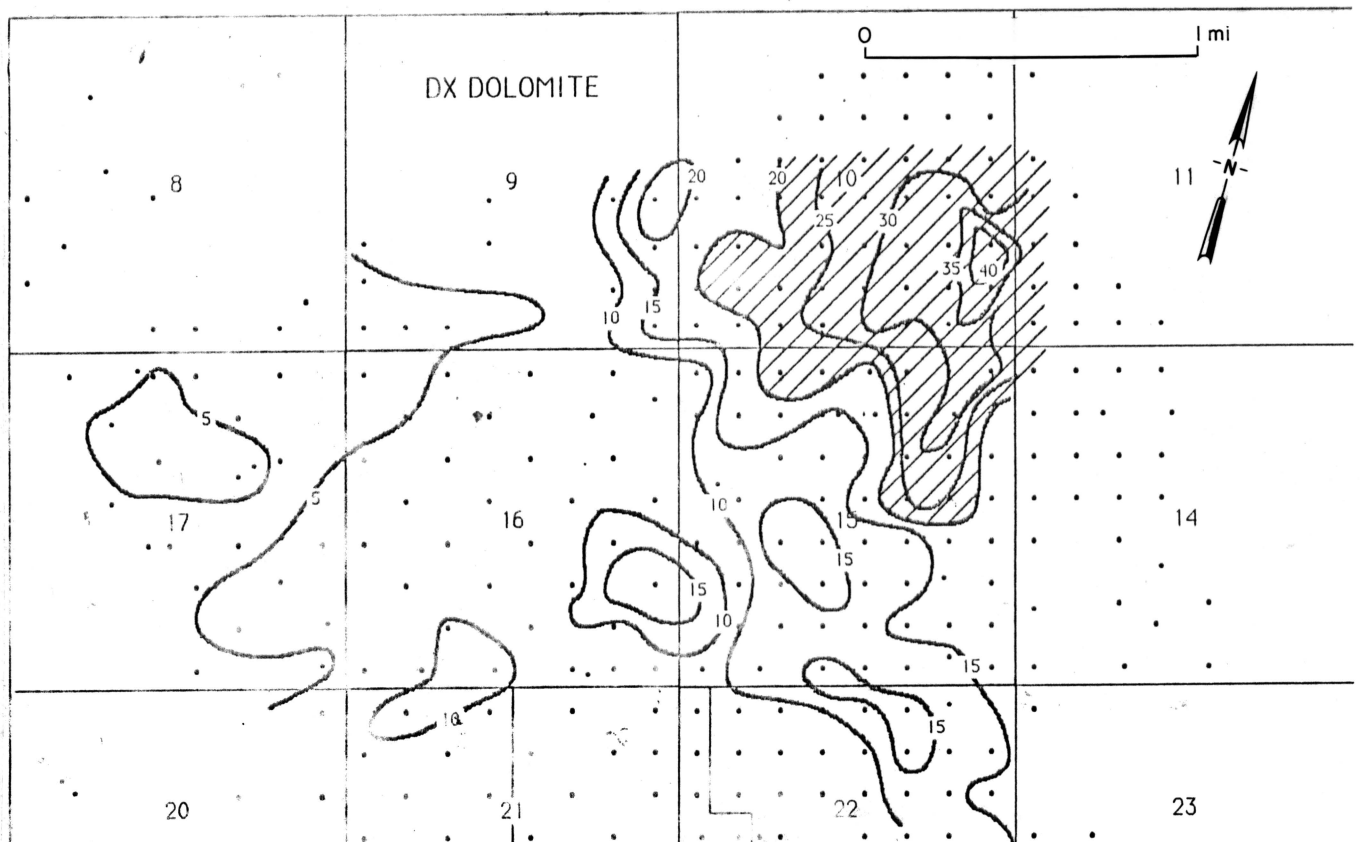


Figure 35. Thickness of the DX Dolomite. The entire area is represented by the pisolite facies.

spaced at the base, become more closely spaced upward in the stratigraphic sequence; consequently, dolomite units thin upward. Each map shows at least part of a facies tract that comprises pisolite grainstone facies on the west, followed to the east by ooid grainstone, pellet grainstone, and fusulinid wackestone. Vertically, this facies tract climbs stratigraphically from west to east. For example, in the lower subdivision (AB) the pisolite grainstone facies occurs on the western side of the mapped area; in contrast, in the upper subdivision (DX) the pisolite grainstone has shifted to the east to extend over the entire area.

### Depositional Environments

The fusulinid wackestone of the lower unit is the most widely distributed facies studied and was recognized in all of the cores of this unit. The abundance of fusulinds, burrows, and carbonate mud suggests deposition in shallow, normal-marine water below wave base in low-energy conditions. A small shoal complex may have developed locally, as suggested by the thin pellet grainstone bed developed at the top of some of the cores. However, high-energy shoals and tidal flats equivalent to this subtidal section are expected to occur to the west toward the interior of the bank.

The middle unit comprises sponge-algal framestone, crinoid-bryozoan packstone, and crinoid-pellet packstone (Fig. 36). The sponge-algal framestone is interpreted to represent a low-energy shallow-water bank of oriented heads composed largely of soft sponges and blue-green algae. Lack of significant hard parts resulted in later partial collapse of the structures and disruption of the vertical alignment. The structures were probably oriented somewhat perpendicular to the tidal energy and focused higher energy tidal currents between them, perhaps similar to the role played by the modern algal structures of Shark Bay. The structures are characterized by abrupt horizontal changes in carbonate textures across the core surfaces. Channels between the sponge-algal structures and tidal deltas basinward of the bank are filled with crinoid-bryozoan packstone. Locally grainstones

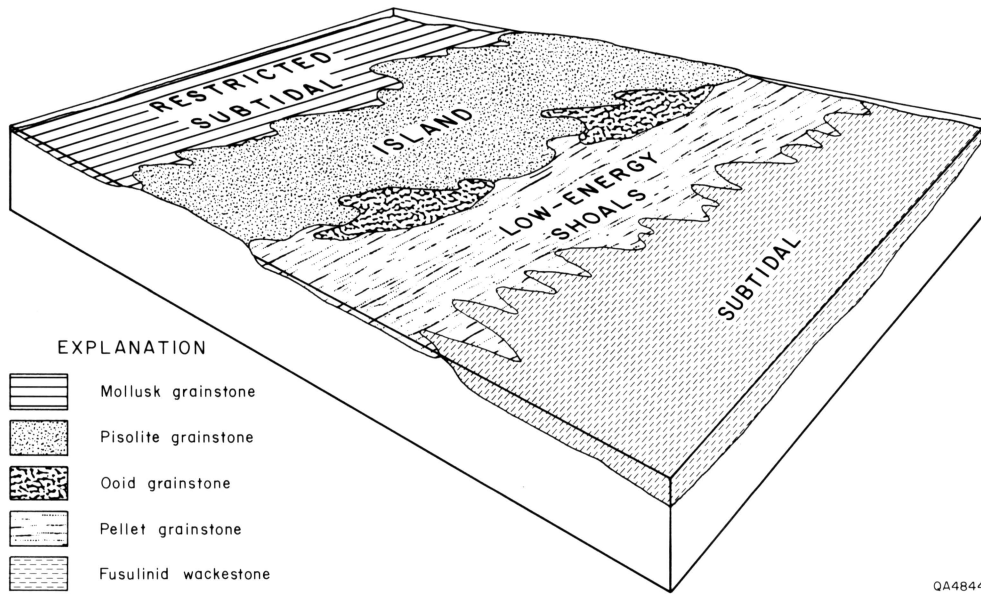


Figure 36. Interpreted depositional environments of the middle unit (MA).

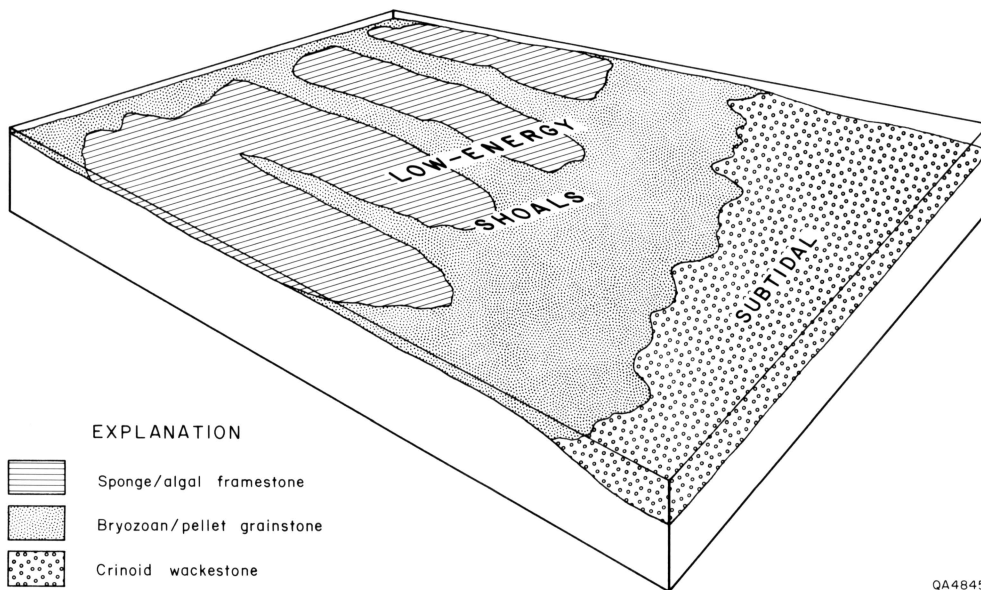


Figure 37. Interpreted depositional environments of the upper unit (A to top of Grayburg).

occur where somewhat stronger currents were focused. Lower energy basinward of the bank and tidal-delta trend is indicated by the more muddy crinoid-pellet packstone facies, which is thought to represent low-gradient slope deposits.

The vertical succession from bottom to top of fusulinid wackestone, pellet grainstone, ooid grainstone, and pisolite grainstone of the upper unit (Fig. 37) is interpreted to represent a progradational sequence from shallow-water subtidal to arid tidal flat conditions, respectively. The pisolite grainstone contains abundant pisolites, sheet and shrinkage cracks, and tepee structures indicative of subaerial environment subjected to severe desiccation. Associated with the pisolite facies are laminated mudstones and algal-laminated mudstones that were probably deposited in restricted ponds on the tidal flat and islands. Highest energy occurred along the edges of these islands where crossbedded and laminated ooids accumulated as fringing bars and beaches. The pellet grainstone, basinward of the ooid facies, represents a broad area of low-energy burrowed stable grain flat with water depths generally below normal wave base. Farther offshore is the extensive shallow-water subtidal shelf in which fusulinid wackestone is the representative facies.

## DIAGENESIS

The following discussion of diagenesis of the San Andres/Grayburg Formations is taken from Leary (1984). Reflux is interpreted to be the dominant mechanism of dolomitization of the San Andres/Grayburg Formations of the eastern Central Basin Platform. Other mechanisms of dolomitization ("sabkha" and schizohaline) were active in the penecontemporaneous diagenetic realm, but probably contributed little to the overall volume of dolomite in the San Andres/Grayburg.

Oxygen-isotope and limited strontium-isotope data support reflux dolomitization by a concentrated brine of late Guadalupian/early Ochoan age. The fluid for dolomitization

could have originated during deposition of the Seven Rivers, Salado, and Rustler Formations. Oxygen isotopes show little variability from micritic to recrystallized microspar and pseudospar dolomite, suggesting recrystallization in a rock-dominated system with an isotopically constant fluid input.

Dolomites with variable luminescence are limited to supratidal and peritidal environments. Early stabilization of supratidal dolomite is indicated by strontium ratios nearly coincident with the age of the samples. However, changes in the strontium content of Permian seawater through possible interaction with Permian clastics may have resulted in a brine capable of imparting a unique strontium isotope signature to early stabilized dolomites.

Dolomite cements in vugs and pores formed from brines with a component of meteoric water. Dolomite cement that lines birdseye vugs is oddly faceted and non-luminescing (Mn- and Fe-free) and is interpreted to have been precipitated in the penecontemporaneous realm of diagenesis. Fringing luminescent cements are interpreted to have precipitated from after deposition to just before cementation by zoned dolomite cements. These larger luminescent dolomite rhomb cements show zoning from dull red to bright orange luminescence that corresponds to an increase in the available manganese to the precipitating carbonate. The source of the manganese is unknown. An iron-rich dolomite cement with a light oxygen isotopic signature is interpreted to have precipitated during late burial diagenesis from a fluid with a component of meteoric water.

The final stage of diagenesis is marked by a close association of slightly undulose dolomite and authigenic quartz, kaolinite, calcite, dedolomite, and minor sulfur. Dissolution of feldspars by acidic meteoric waters is presumed to have been the source of the kaolinite, although albitization of calcic plagioclase has not been discounted as a source of aluminum in the subsurface. Sulfate-reducing bacteria, borne by continental ground waters, reduce sulfate and oxidize hydrocarbons to give rise to authigenic calcite, dedolomite, and minor sulfur. Recrystallization of dolomite in the presence of reduced

sulfate is thought to give rise to slightly undulose dolomite patches and cements. Oxygen isotopes indicate calcite precipitation either from meteoric water in an open system or from bicarbonates constructed with light-sulfate oxygen in a closed system.

### Porosity/Permeability

Four pore types are recognized in the dolomite facies of the San Andres/Grayburg Formations--vuggy, moldic, interparticle, and dolomite intercrystalline. The highest porosity and permeability were found in the thin pellet grainstones; thicker sections of consistent but slightly lower porosity and permeability occur in the mud-dominated facies, such as the fusulinid wackestone. However, even in the wackestone facies the areas of higher porosity and permeability have a slightly higher grain content.

There is a considerable difference in the type of porosity and its distribution between the eastern and western halves of the study area (Fig. 23). In the eastern half of the study area, porosity and permeability are best developed (up to 20 percent porosity and 100 md permeability) in the pellet grainstone of the CZ dolomite. The underlying fusulinid wackestone between the A and C markers is considerably thicker and contains 5 to 10 percent porosity and lower, more variable permeability from 0.1 to 100 md. Below the A marker, porosity and permeability are lower in the crinoid-bryozoan packstone and crinoid-pellet packstone facies.

In the western half of the area, porosity is not developed above the A marker. Porosity is greatest in the sponge-algal framestone facies between A and M markers where it reaches 14 percent; permeability ranges from 0.2 to 0.5 md. Although lower, this thick section of sponge-algal framestone has considerably less variation of porosity and permeability than does the fusulinid wackestone to the east. The eastern and western halves of the area therefore appear to be two separate reservoirs. The eastern half produces primarily from the upper part between the A and Z markers; the western half, on the other hand, produces from the lower part between the M and A markers.

Porosity distribution charts aid in the characterization of the porosity within each facies by demonstrating the percent of the thickness represented at each porosity level. In the upper unit, the pellet grainstone (Fig. 38) is characterized by symmetrical distribution of between 12 and 20 percent porosity and an average peak at 16 percent in the eastern part of the area; the less porous pellet grainstone to the west displays a wide distribution of 2 to 24 percent and an average indefinite peak at 10 to 12 percent. The ooid grainstone (Fig. 39), in contrast, shows a narrow distribution of 4 to 8 percent; average porosity is 6 percent. In between, in a mixed ooid/pellet grainstone transition, the porosity distribution shows both a low-porosity ooid peak and a higher porosity pellet peak. The closely associated fusulinid wackestone (Fig. 40) has a broad distribution of 4 to 18 percent and an average of 8 to 10 percent. In the middle unit the sponge-algal framestone (Fig. 41) on the western side of the area has an extremely narrow distribution of 10 to 14 percent and an average of 12 percent porosity. To the east, the equivalent crinoid-bryozoan-pellet facies (Fig. 42) shows a wide distribution of 4 to 20 percent porosity and an average of 12 percent. However, when the two subfacies are separated, it is obvious that the most porosity is in the crinoid-bryozoan packstone facies, where it ranges from 6 to 20 percent and averages 14 percent. The crinoid-pellet packstone facies has porosity ranging only from 4 to 16 percent and an average of 10 percent.

Porosity/permeability plots (Figs. 43 through 46) were made of all facies that have more than 0.1 md permeability. The plots show considerable scatter. Data from the pellet grainstone facies (Fig. 43) show the tightest clusters and consistently highest permeability (10 to 100 md) of all of the facies. However, no relationship to porosity is obvious. The sponge-algal framestone facies (Fig. 44) shows the lowest permeability of all the productive facies as it does not exceed 1 md and has no obvious correlation with porosity. The data from the crinoid/bryozoan packstone facies (Fig. 45) and fusulinid wackestone facies (Fig. 46) show similar scatter with the fusulinid wackestone facies having a few more data points in the 10 to 100 md range. Here, there is a general relationship with

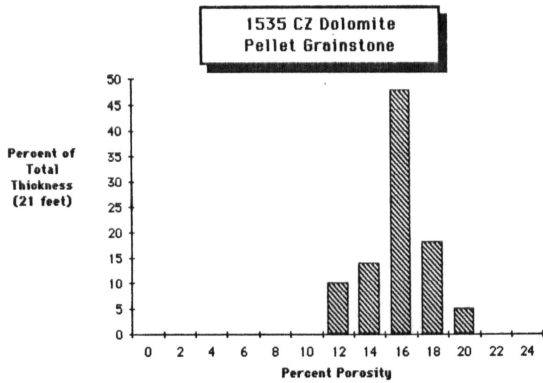


Figure 38. Porosity distribution of the pellet grainstone of the CZ Dolomite in the Mobil University #1535.

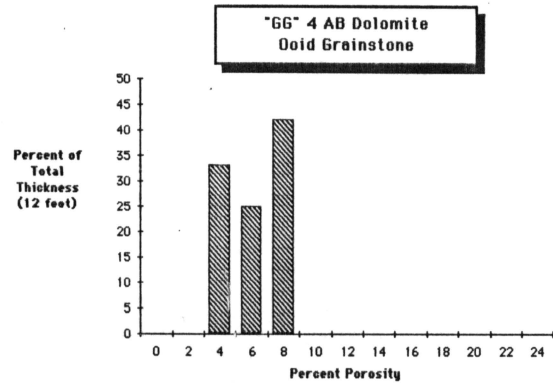


Figure 39. Porosity distribution of the ooid grainstone of the AB Dolomite in the Mobil University #GG4.

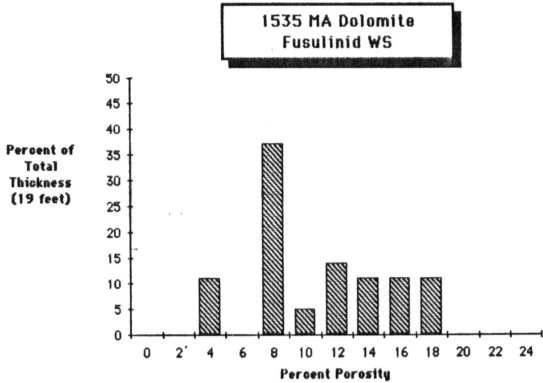


Figure 40. Porosity distribution of the fusulinid wackestone of the MA Dolomite in the Mobil University #1535.

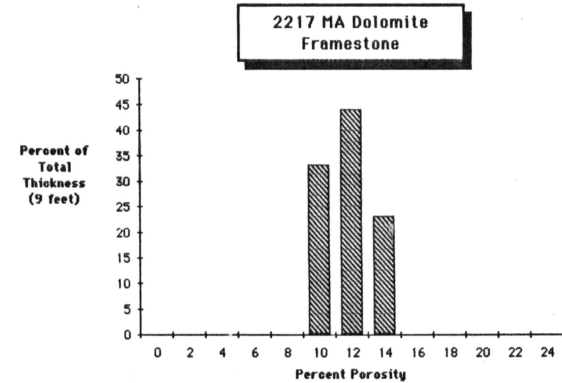


Figure 41. Porosity distribution in the algal framestone of the MA Dolomite in the Getty #2217.

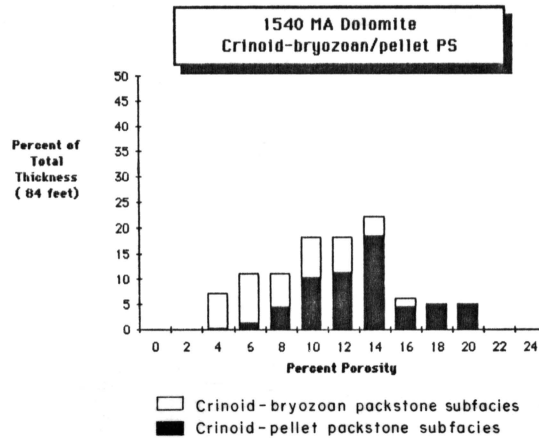


Figure 42. Porosity distribution of the crinoid-bryozoan packstone (white) and crinoid-pellet packstone (black) of the MA Dolomite in the Mobil University #1540.

porosity but nothing predictable. These porosity/permeability plots are typical of carbonate reservoirs and illustrate the problems inherent in attempting to relate permeability or fluid-flow properties to rock facies. More detailed work must be done to refine these relationships.

#### PRODUCTION STUDIES -- DUNE FIELD UNIT 15/16

Statistics of oil and water production and water injection at the Mobil Unit 15/16 from January 1977 to September 1984 have been subdivided for analysis into old wells (drilled prior to 1958) and new wells (drilled since 1978). The map of cumulative production from the old wells (Fig. 47) shows a dominant northwest-southeast trend, decidedly similar to the facies trends of the AB (Fig. 28), BC (Fig. 29), CZ (Fig. 30), and ZY (Fig. 32) correlation units. This trend is not as clear on the cumulative production from the new wells (Fig. 48).

All wells have produced some water since early in their production history, and since water injection began in 1978, there has been a decided increase in water production rates from most wells near injection wells (Fig. 49). Oil production increases, on the other hand, have been negligible.

Figures 50 and 51 illustrate the production behavior of two wells, #1520 (Fig. 51) and #1531 (Fig. 50), together with water-injection data on nearby water-injection wells. Well #1531 is the only well examined to date that indicated any benefit from water injection. However, there has been no fill-up of the reservoir by water injection; in fact, only slightly more water has been injected than has been produced. It appears that injection water is bypassing oil to reach the producing well.

PERMEABILITY-POROSITY CROSS PLOT  
(CORE ANALYSIS)  
PELLET GRAINSTONE FACIES

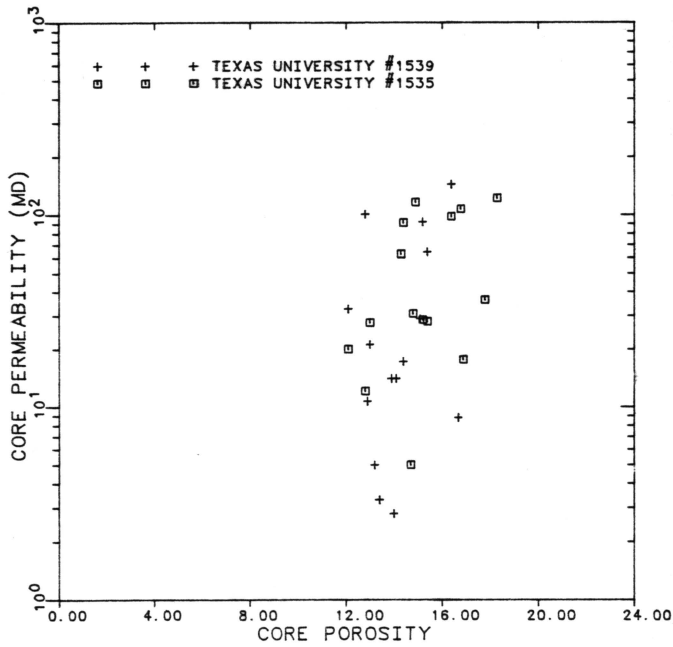


Figure 43. Porosity/permeability cross plot of the pellet grainstone facies.

PERMEABILITY-POROSITY CROSS PLOT  
(CORE ANALYSIS)  
FRAMESTONE FACIES

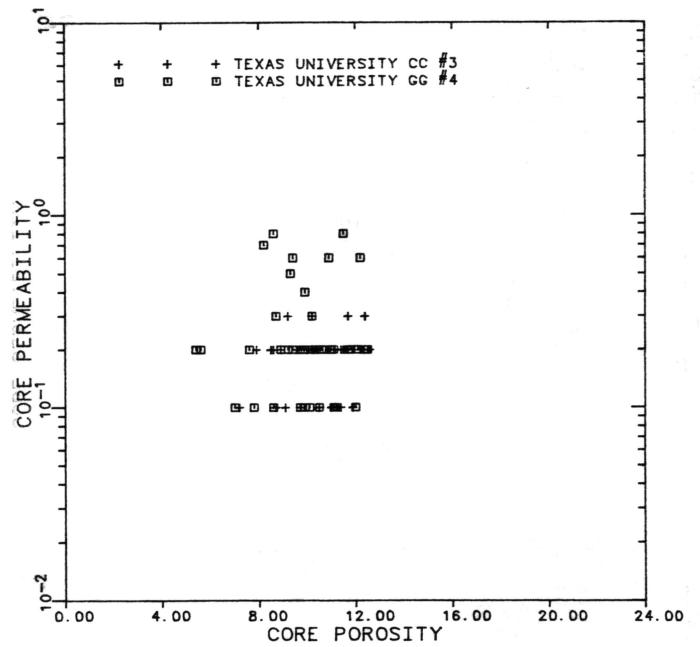


Figure 44. Porosity/permeability cross plot of the sponge-algal framestone facies.

PERMEABILITY-POROSITY CROSS PLOT  
(CORE ANALYSIS)  
CRINOID/BRYOZOAN PACKSTONE FACIES

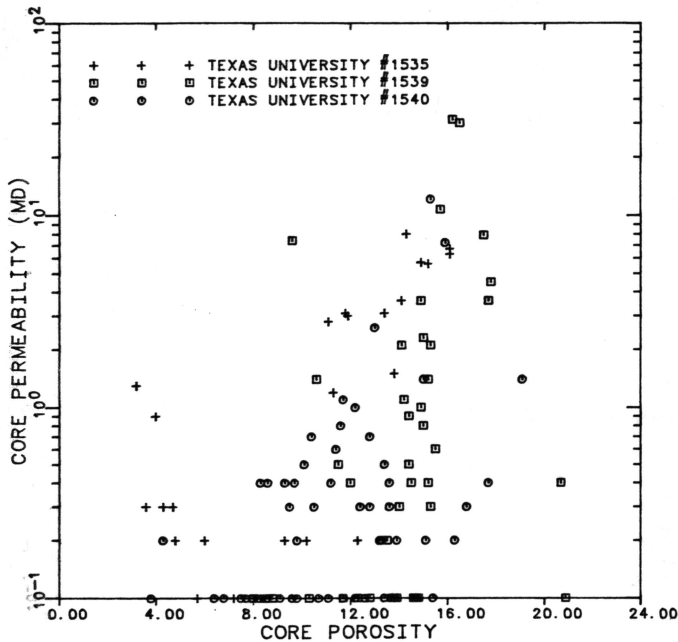


Figure 45. Porosity/permeability cross plot of the crinoid-bryozoan packstone facies.

PERMEABILITY-POROSITY CROSS PLOT  
(CORE ANALYSIS)  
FUSULINID WACKSTONE FACIES

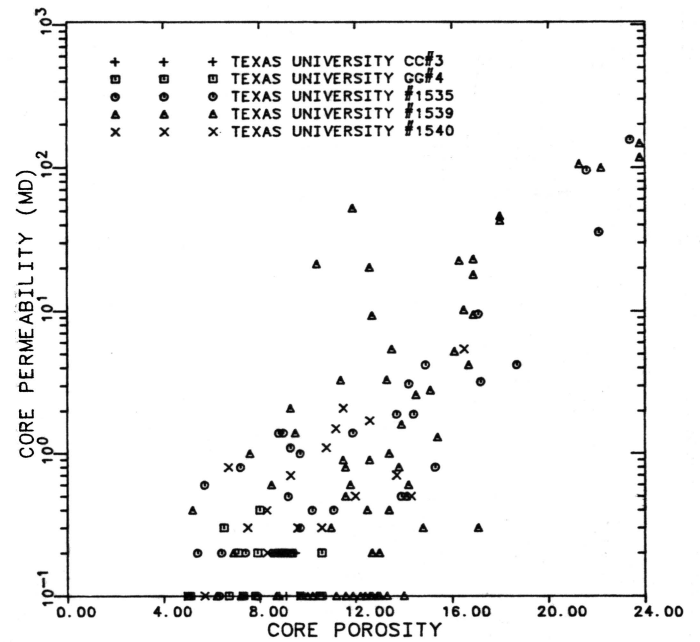


Figure 46. Porosity/permeability cross plot of the fusulinid wackstone facies.

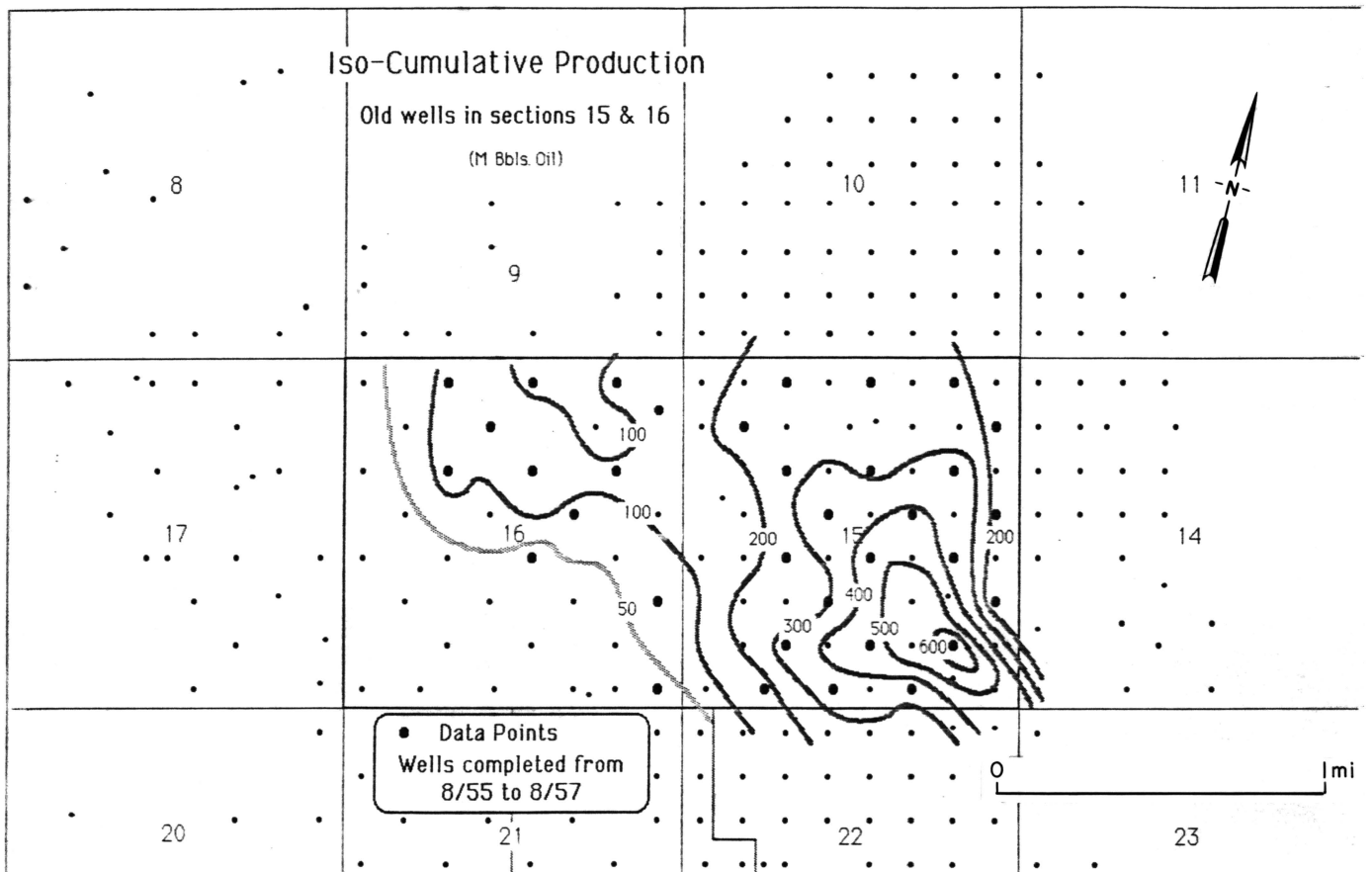


Figure 47. Cumulative production from wells drilled prior to 1958 in sections 15 and 16.

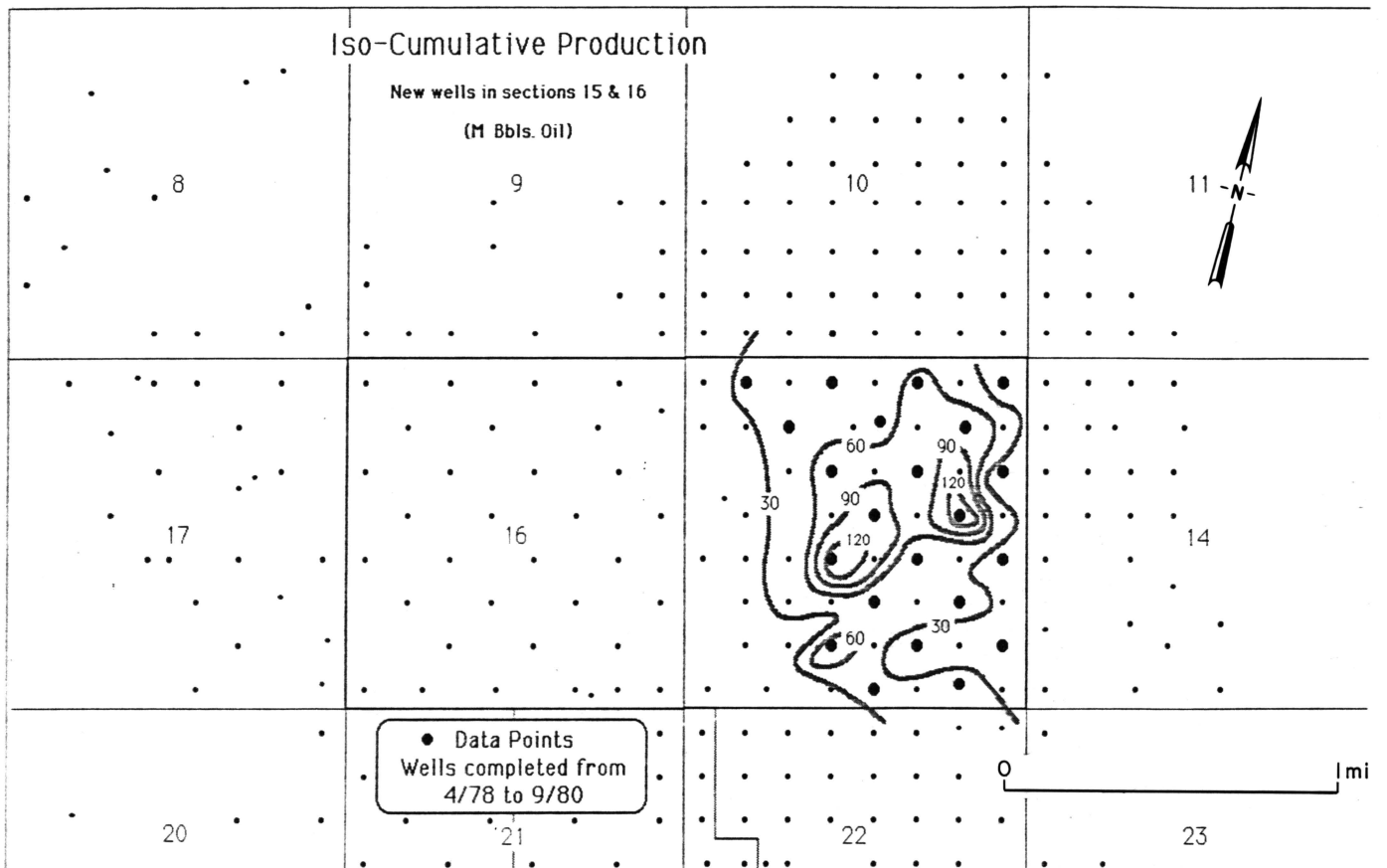


Figure 48. Cumulative production from wells drilled since 1958.

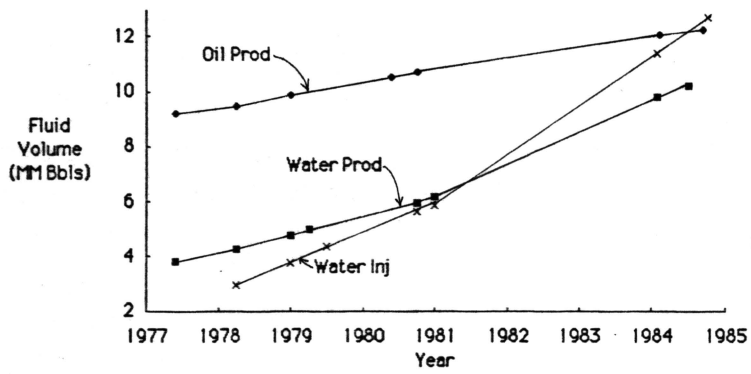


Figure 49. Cumulative production of oil and water and volume of water injected from 1977 to 1985 from wells in sections 15 and 16.

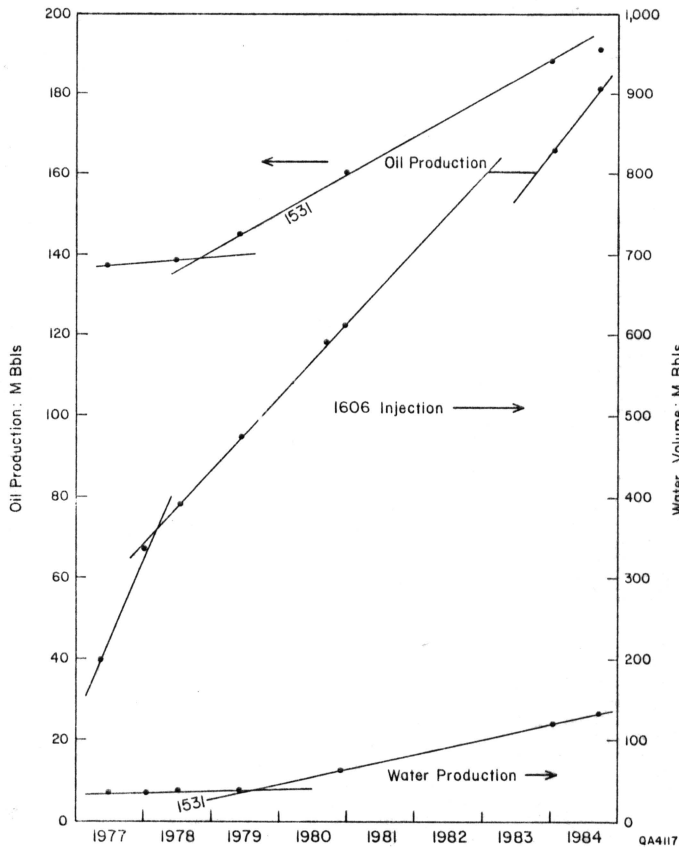
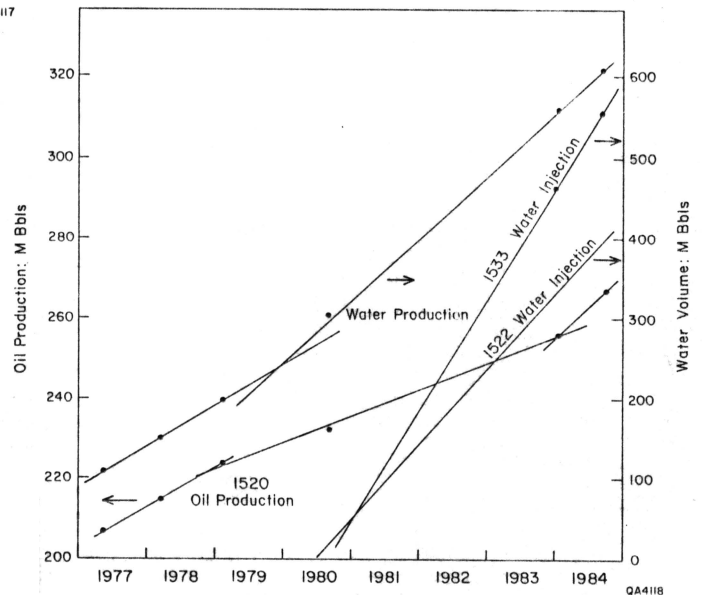


Figure 50. Production behavior of Mobil University #1531 and water injection in a nearby well.

Figure 51. Production behavior of Mobil University #1520 and water injection in a nearby well.



## CONCLUSIONS

From this study of cores and logs from the Mobil University Unit 15/16 and nearby areas of the Dune Field, eight dolomite and one siltstone facies have been recognized within the producing section of the San Andres/Grayburg Formations. Within any time-equivalent zone, facies change from one side of the study area to the other. In spite of the extensive dolomitization it is possible to relate the present porosity to controls by depositional facies. Therefore, the porosity distribution is predictable.

Within the framework of a detailed correlation grid based on siltstone correlations, the eastern half of the area in section 15 has the best porosity development in the upper part of the perforated section; the highest porosity is preserved in the pellet grainstone. High initial potentials of many wells suggest that early production was from this highly porous and permeable zone. The lower, more sustained production is from the less porous and permeable fusulinid wackestone. To the west in section 16, the upper part of the comparable section comprises pisolite and ooid grainstone facies and is nonporous. Production to the west is from lower in the perforated section from the sponge-algal framestone, as the pellet grainstone to the west is cemented with anhydrite.

The nature of the porosity within each facies is displayed in the porosity-distribution charts. Although there is some overlap, each facies has a recognizable pattern, and in the absence of cores these charts can be used as an aid in identifying the facies. Various log cross-plotting methods have also aided in the recognition of the facies locally.

There is a positive correlation between the cumulative oil production and more favorable reservoir facies. However, limited injection data indicate that water injection has resulted in negligible increases in oil production; fill-up of the reservoir has not been achieved and injected water appears to be bypassing the oil to reach producing wells. Additional study of this unit will focus on application of additional production data to the geological framework.

## REFERENCES

- Babcock, J. A., 1977, Calcareous algae, organic boundstones, and genesis of the upper Capitan Limestone (Permian, Guadalupian), Guadalupe Mountains, West Texas and New Mexico: in Hileman, M. E., and Mazzullo, S. J., eds., Upper Guadalupian facies, Permian reef complex, Guadalupe Mountains, New Mexico and West Texas: S.E.P.M. Permian Basin Section Pub. 77-16, p. 17-39.
- Crawford, G. A., 1981, Depositional history and diagenesis of the Goat Seep Dolomite (Permian, Guadalupian), Guadalupe Mountains, West Texas - New Mexico: Univ. of Wisconsin, Madison, Ph.D. dissertation, 300 p.
- Galloway, W. E., Ewing, T. E., Garrett, C. M., Tyler, N., and Bebout, D. G., 1983, Atlas of major Texas oil reservoirs: The University of Texas at Austin, Bureau of Economic Geology, Special Publication, 139 p.
- Hills, J. M., 1972, Late Paleozoic sedimentation in West Texas Permian basin: American Association of Petroleum Geologists Bulletin, v. 56, p. 2303-2322.
- Leary, D. A., 1984, Diagenesis of the Permian (Guadalupian) San Andres and Grayburg Formations, Central Basin Platform, West Texas: The University of Texas at Austin, Master's thesis, 129 p.
- Longacre, S. A., 1980, Dolomite reservoirs from Permian biomicrites, in Halley, R. B., and Loucks, R. G., eds., Carbonate Reservoir Rocks: S.E.P.M. Core Workshop No. 1, p. 105-117.
- \_\_\_\_\_ 1983, A subsurface example of a dolomitized Middle Guadalupian (Permian) reef from West Texas, in Harris, P. M., ed., Carbonate buildups -- a core workshop: S.E.P.M. Core Workshop No. 4, p. 304-326.
- Toomey, D. F., and Cys, J. M., 1979, Community succession in small bioherms of algae sponges in the lower Permian of New Mexico: Lethaia, v. 12, p. 65-74.

Yurewicz, D. A., 1977, Origin of the massive facies of the lower and middle Capitan Limestone (Permian), Guadalupe Mountains, New Mexico and West Texas, in Hileman, M. E., and Mazzullo, S. J., eds., Upper Guadalupian facies, Permian reef complex, Guadalupe Mountains, New Mexico and West Texas: S.E.P.M. Permian Basin Section, Pub. 77-16, p. 45-92.

- Figure 1. Estimated original oil in place in Texas. More than 50 percent is from the Permian Basin.
- Figure 2. Cumulative production of oil from Texas through 1982.
- Figure 3. Cumulative production of oil from the Permian Basin through 1982, showing the dominance of carbonate reservoirs.
- Figure 4. Cumulative production of oil from carbonate reservoirs through 1982. San Andres/Grayburg reservoirs account for almost half of the production from carbonate reservoirs.
- Figure 5. Principal Paleozoic oil-bearing units of North and West Texas. From Galloway et al. (1983).
- Figure 6. Location of the cross section across the Central Basin Platform.
- Figure 7. Structural cross section across the Central Basin Platform.
- Figure 8. Location of University Lands in the Permian Basin.
- Figure 9. San Andres/Grayburg fields, Permian Basin, Texas.
- Figure 10. Outline of Dune Field showing the location of the study area in University Lands Block 30.
- Figure 11. Well log and core (numbered large dots) control in the study area comprising the Mobil University Unit 15/16 and adjoining sections.
- Figure 12. Structure on the top of the Grayburg Formation (Fig. 15).
- Figure 13. Cumulative production through 1982 from sections 15 and 16.
- Figure 14. Initial-potential map prepared using older wells drilled prior to waterflooding.
- Figure 15. Gamma ray/sonic log of the San Andres, Grayburg, and Queen section in the Mobil University No. 1557.
- Figure 16. Index map of the study area showing the location of the log correlation cross sections.
- Figure 17. Pisolite grainstone facies comprising pisolite grainstone (a, b), laminated mudstone (c), and algal laminated mudstone (d) facies. Slabbed surfaces.
- Figure 18. Ooid and pellet grainstone facies.
- a. Crossbedded ooid grainstone. Slabbed surface.
  - b. Ooid grainstone. Thin section, X20, from Mobil University No. CC3, 3,139 feet.
  - c. Burrowed pellet grainstone. Slabbed surface.
  - d. Pellet grainstone. Thin section, X20, from Mobil University No. 1539, 3,337 feet.
- Figure 19. Fusulinid wackestone facies.
- Figure 20. Sponge-algal framestone facies.

Figure 21. Siltstone facies.

Figure 22. Index map of the study area showing location of the detailed facies cross section.

Figure 23. Detailed facies cross section. Location of section is shown in Figure 22.

Figure 24. Cross plot of neutron porosity vs. resistivity using wells from the west half of the study area. The various facies as identified from core examination are indicated by the different symbols.

Figure 25. Cross plot of sonic travel time vs. neutron porosity using wells from the east half of the study area. The various facies as identified from core examination are indicated by the different symbols.

Figure 26. Thickness of the MA Dolomite. The facies represented in this unit are indicated by the hachures.

Figure 27. Thickness of the A Siltstone. Although this siltstone extends throughout the study area only the thicker part is indicated by the hachures.

Figure 28. Thickness of the AB Dolomite. The facies represented in this unit are indicated by the hachures.

Figure 29. Thickness of the BC Dolomite. The facies represented in this unit are indicated by the hachures.

Figure 30. Thickness of the CZ Dolomite. The facies represented in this unit are indicated by the hachures.

Figure 31. Thickness of the Z Siltstone.

Figure 32. Thickness of the ZY Dolomite. The facies represented in this unit are indicated by the hachures.

Figure 33. Thickness of the Y Siltstone. The thicker areas are indicated by the hachures.

Figure 34. Thickness of the YD Dolomite. The facies represented in this unit are indicated by the hachures.

Figure 35. Thickness of the DX Dolomite. The entire area is represented by the pisolite facies.

Figure 36. Interpreted depositional environments of the middle unit (MA).

Figure 37. Interpreted depositional environments of the upper unit (A to top of Grayburg).

Figure 38. Porosity distribution of the pellet grainstone of the CZ Dolomite in the Mobil University #1535.

Figure 39. Porosity distribution of the ooid grainstone of the AB Dolomite in the Mobil University #GG4.

Figure 40. Porosity distribution of the fusulinid wackestone of the MA Dolomite in the Mobil University #1535.

Figure 41. Porosity distribution in the algal framestone of the MA Dolomite in the Getty #2217.

Figure 42. Porosity distribution of the crinoid-bryozoan packstone (white) and crinoid-pellet packstone (black) of the MA Dolomite in the Mobil University #1540.

Figure 43. Porosity/permeability cross plot of the pellet grainstone facies.

Figure 44. Porosity/permeability cross plot of the sponge-algal framestone facies.

Figure 45. Porosity/permeability cross plot of the crinoid-bryozoan packstone facies.

Figure 46. Porosity/permeability cross plot of the fusulinid wackestone facies.

Figure 47. Cumulative production from wells drilled prior to 1958 in sections 15 and 16.

Figure 48. Cumulative production from wells drilled since 1958.

Figure 49. Cumulative production of oil and water and volume of water injected from 1977 to 1985 from wells in sections 15 and 16.

Figure 50. Production behavior of Mobil University #1531 and water injection in a nearby well.

Figure 51. Production behavior of Mobil University #1520 and water injection in a nearby well.